

DEVELOPMENT OF UNMANNED AERIAL VEHICLE (UAV)
FOR WILDLIFE SURVEILLANCE

By

KYUHO LEE

A THESIS PRESENTED TO THE GRADUATE SCHOOL
OF THE UNIVERSITY OF FLORIDA IN PARTIAL FULFILLMENT
OF THE REQUIREMENTS FOR THE DEGREE OF
MASTER OF SCIENCE

UNIVERSITY OF FLORIDA

2004

Copyright 2004

by

KYUHO LEE

*To my parents, wife, and daughter,
In – myoung Park, Pan-hyi Lee, Nanyoung Seo, and Eugenia Lee.*

ACKNOWLEDGMENTS

I have many people to thank for their assistance. I have confronted many difficulties during my academic career. However, I could not have overcome such difficulties without their support and help. In particular I am greatly indebted to my adviser, Dr. Peter Ifju, for providing me with the means and opportunity to work on this project. I would like to recognize Dr. Percival Franklin for all of his invaluable support. I also wish to thank my colleagues who have worked with me: Paul Barnswell, who was always a good friend and advisor; Sewoong Jung, who helped me adjust to life in America; Dragos Veiiu, who gave the best guide to CFD simulation; Danial Grant, who offered valuable help for building an airplane; Bret Stanford and Mike Sytsma, who were great contributors to designing and fabricating the air plane; Frank Boria, who has shared MAV research enthusiasm; Scott Bowman, who has assisted with testing the airplane, and Jangyoung Huh, who has spent considerable time assisting with thesis editing.

To my family, I would like to say “I love you” rather than “thank you.” I love my mother, I love my daughter, Eugin, I love my wife, Nanyoung. I am glad to dedicate my thesis to them.

TABLE OF CONTENTS

| | <u>page</u> |
|------------------------------------------------------------|-------------|
| ACKNOWLEDGMENTS | iv |
| LIST OF TABLES | viii |
| LIST OF FIGURES | ix |
| ABSTRACT | xiii |
| CHAPTER | |
| 1 INTRODUCTION | 1 |
| 1.1 Various Unmanned Aerial Vehicles | 1 |
| 1.2 Small Unmanned Aerial Vehicles (SUAV) | 2 |
| 1.3 Motivation of Development | 3 |
| 1.4 Thesis Objective | 4 |
| 1.5 Design Metrics | 4 |
| 1.6 Related Work | 5 |
| 1.7 Technical Challenge | 5 |
| 2 WSUAV REQUIREMENTS | 6 |
| 2.1 Mission Profile and Overview | 6 |
| 2.2 Design Requirements | 8 |
| 3 DESIGN OF WSUAV | 10 |
| 3.1 Consideration to Wildlife Application and Design | 10 |
| 3.2 Design Process | 11 |
| 3.3 Wing Design | 11 |
| 3.3.1 Plan form Design | 13 |
| 3.3.2 Wing area and Airfoil estimation | 15 |
| 3.3.3 Airfoil Design | 17 |
| 3.3.4 Aerodynamic Calculation | 18 |
| 3.3.5 Computer Fluid Dynamics (CFD) Simulation | 21 |
| 3.3.6 Wind Dihedral | 23 |
| 3.4 Fuselage Design | 25 |

| | | |
|-------|--------------------------------------------------------------|----|
| 3.4.1 | Structural Cosiderations | 25 |
| 3.4.2 | Consideration of Center of Gravity (CG) | 26 |
| 3.4.3 | Lift-Dependent Drag-Factor, C_{Di} | 27 |
| 3.4.4 | Consideration of Hatch Design | 28 |
| 3.5 | Stabilizer Design | 28 |
| 3.6 | Propulsion system | 32 |
| 3.6.1 | Electric Motor Selection | 33 |
| 3.6.2 | Cooling Consideration | 34 |
| 3.6.3 | Battery Selection | 35 |
| 4 | AIRPLANE FABRICATION | 37 |
| 4.1 | Wing Fabrication | 37 |
| 4.2 | Fuselage Fabrication | 41 |
| 4.3 | Stabilizers Fabrication | 43 |
| 5 | AVIONICS | 47 |
| 5.1 | Avionics Configuration | 47 |
| 5.2 | Kestrel Autopilot System | 50 |
| 5.2.1 | Autopilot Control Theory | 52 |
| 5.2.2 | The Virtual Cockpit Software | 55 |
| 5.3 | Camera and Recording System | 56 |
| 5.4 | Ground Plane (GP) Antenna Design for Video Transmitter | 59 |
| 5.5 | Video Reception Maximization at the Ground Station | 64 |
| 5.6 | Camera Switching Device Design and Fabrication | 67 |
| 6 | AIRPLANE EVALUATION | 69 |
| 6.1 | Propulsion Evaluation | 70 |
| 6.1.1 | Comparison of Climb Rate at Take Off | 70 |
| 6.1.2 | Comparison of Efficiency at Cruise | 72 |
| 6.2 | Autopilot Evaluation | 76 |
| 7 | CONCLUSION | 79 |
| 7.1 | Conclusion | 79 |
| 7.2 | Future Recommendation | 79 |
| | APENDIX | 80 |
| A | LKH2411 AIRFOIL COORDINATES | 80 |
| B | LKH 2411 SIMULATION DATA | 82 |
| C | EH 00/90 AIRFOIL COORDINATES | 84 |

| | |
|---------------------------|----|
| LIST OF REFERENCES | 85 |
| BIOGRAPHICAL SKETCH | 87 |

LIST OF TABLES

| <u>Table</u> | <u>page</u> |
|--------------------------------------------------------------------|-------------|
| 1-1 The wingspan and flying time of the SUAV are compared | 3 |
| 2-1 Design requirements | 8 |
| 2-2 WSUAV design objectives and constraints comparing SUV | 9 |
| 3-1 W/S comparison with other SUAVs..... | 14 |
| 3-2 WSUAV weight distribution, W (3.371 kg)..... | 15 |
| 3-3 T/W comparison with other SUAVs | 19 |
| 3-4 CFD flows and pressure visualizations results comparison | 23 |
| 3-5 Tested stabilizer specifications | 30 |
| 3-6 Specification of electric motor | 34 |
| 3-7 Specifications of selected battery | 36 |
| 5-1 Electric devices in the avionics | 49 |
| 5-2 Cameras specification as shown in Figure 5.12 and 5.13..... | 57 |
| 5-3 Antennas comparison of output power | 65 |

LIST OF FIGURES

| <u>Figure</u> | <u>page</u> |
|-----------------------------------------------------------------------------------|-------------|
| 1-1 UAVs can be divided into four groups by respect to its sizes and weights..... | 2 |
| 2-1 Oscillating path survey | 6 |
| 2-2 Random path survey | 6 |
| 2-3 Diagram used to calculate the field of view of a camera view angle | 7 |
| 2-4 Typical WSUAV's mission profile | 8 |
| 3-1 Design and manufacturing process..... | 11 |
| 3-2 Elliptical wing platform shape comparison..... | 12 |
| 3-3 Typical effect of aspect ratio on lift..... | 12 |
| 3-4 LKH 2411 Airfoil at 2.5° AOA..... | 17 |
| 3-5 C_l vs AOA for LKH 2411 & NACA 2411 | 17 |
| 3-6 C_d vs AOA for LKH 2411 & NACA2411 | 17 |
| 3-7 C_l/C_d vs AOA for LKH 2411 & NACA 2411 | 17 |
| 3-8 C_m vs AOA for LKH 2411 & NACA 2411 | 17 |
| 3-9 LKH 2411 C_l vs C_d | 20 |
| 3-10 Tested wing platform comparison | 21 |
| 3-11 CFD simulation for design one..... | 22 |
| 3-12 Vorticity simulation for design one | 22 |

| | |
|------------------------------------------------------------------------|----|
| 3-13 CFD simulation for design two | 22 |
| 3-14 Vorticity simulation for design two..... | 22 |
| 3-15 CFD simulation for design three | 23 |
| 3-16 Vorticity simulation for design three..... | 23 |
| 3-17 The final design of the right wing | 25 |
| 3-18 Payload distribution in the fuselage..... | 27 |
| 3-19 Lift-dependent factor for fuselage interface | 28 |
| 3-20 Tested stabilizer configurations..... | 30 |
| 3-21 Side view | 31 |
| 3-22 Top view | 32 |
| 3-23 Front view..... | 32 |
| 3-24 Optimum condition of propulsion system | 33 |
| 3-25 Gravimetric energy density in various batteries | 35 |
| 4-1 Master wing shape (right side) for the creating mold..... | 38 |
| 4-2 Female molds for the wings..... | 39 |
| 4-3 Wing manufacturing layout..... | 40 |
| 4-4 Before wing assembly | 41 |
| 4-5 Assembled wing and joint pipe | 41 |
| 4-6 Female molds for the fuselage..... | 42 |
| 4-7 Fabricated fuselage..... | 43 |
| 4-8 Fabricated stabilizer..... | 45 |
| 4-9 Disassembled modular parts fit into the one man carrying box | 45 |
| 4-10 Assembled final design WSUAV | 46 |
| 5-1 WSUAV avionics configuration..... | 48 |
| 5-2 Kestrel autopilot system | 50 |

| | | |
|------|-----------------------------------------------------------------------------|----|
| 5-3 | Kestrel autopilot | 51 |
| 5-4 | Kestrel autopilot ground station | 51 |
| 5-5 | Roll rate controller and inner lateral roll | 53 |
| 5-6 | Outer lateral heading angle controller | 53 |
| 5-7 | Inner longitudinal pitch and pitch controller | 54 |
| 5-8 | Inner longitudinal airspeed controller..... | 54 |
| 5-9 | Outer longitudinal altitude controller | 55 |
| 5-10 | Outer longitudinal airspeed controller..... | 55 |
| 5-11 | The virtual cockpit software | 58 |
| 5-12 | 500 lines resolution CCD camera for the bottom view | 57 |
| 5-13 | 380 lines resolution CCD camera for the side view | 58 |
| 5-14 | Video recording device..... | 58 |
| 5-15 | Comparison of antenna radiation pattern..... | 60 |
| 5-16 | Fabricated and calibrated GP antenna | 61 |
| 5-17 | Network analyzer showing impedance matching for the GP antenna..... | 63 |
| 5-18 | The Spectrum analyzer output before and after use of customized LNA | 64 |
| 5-19 | Model A2.45FP12 antenna with a customized LNA..... | 65 |
| 5-20 | Schematic diagram of a video transmission | 66 |
| 5-21 | Camera switching device schematic..... | 68 |
| 5-22 | Assembled camera switching device..... | 68 |
| 5-23 | Printed circuit board layout | 68 |
| 6-1 | Takeoff profile with APC9x6E propeller | 70 |
| 6-2 | Takeoff profile with APC10x7E propeller | 71 |
| 6-3 | Airplane's altitude and flight speed variation with APC9x6E propeller..... | 73 |
| 6-4 | Airplane's altitude and flight speed variation with APC10x7E propeller..... | 74 |

| | | |
|------|--------------------------------------------------------------------------------------|----|
| 6-5 | Propeller efficiency of APC 9·6E | 75 |
| 6-6 | Propeller efficiency of APC 10·7E | 75 |
| 6-7 | Closed loop lateral response to step in desired roll angle (Φ)..... | 76 |
| 6-8 | Closed loop longitudinal response to step in desired pitch angle (Θ). | 77 |
| 6-9 | Plan view of autonomous flight to programmed waypoints..... | 78 |
| 6-10 | Altitude and velocity holding during autonomous waypoint navigation | 78 |

Abstract of Thesis Presented to the Graduate School
of the University of Florida in Partial Fulfillment of the
Requirements for the Degree of Master of Science

DEVELOPMENT OF UNMANNED AERIAL VEHICLE (UAV)
FOR WILDLIFE SURVEILLANCE

By

Kyuho Lee

December 2004

Chair: Peter G. Ifju

Major Department: Mechanical and Aerospace Engineering

This thesis presents the design, fabrication, capabilities, and analysis of an autopilot capable Small UAV with a wingspan of fewer than 2 meters for wildlife surveillance.

The highly autonomous flight control system has two high resolution cameras and an onboard video recording device, which collects high quality imagery with specified GPS points and altitudes. Innovative robust construction coupled with light weight and inexpensive hardware was used in the design of the airframe and avionics. These features allow the airplane to be operated by unskilled users.

CHAPTER 1 INTRODUCTION

1.1 Various Unmanned Aerial Vehicles

Unmanned Aerial Vehicles (UAVs) have proven their usefulness in military reconnaissance in recent military conflicts [1]. Their practical applications have been expanding to more than military uses [2]. Various sizes of UAVs are designed to different levels of performance depending on their application. UAVs can be categorized into four different groups: large, medium, small, and micro as shown in Figure 1.1.

Most of the large UAVs have higher flight ceiling, speed, and endurance with more functional capabilities than small UAVs. The representative large UAVs are Northrop Grumman Global Hawk (20m wingspan) [3] and General Dynamics Predator (14.8m wingspan) [3]. They have proven their performance in recent missions. Large UAVs are more suitable for large land or over-water surveillance. The effectiveness of large UAVs has been proven in the Gulf War and Desert Storm.

The representative mid-size UAVs are AAI Shadow (3.9 m wingspan) [5] and IAI Malat Hunter (8.8 m wingspan) [5]. Most mid-size UAVs do not require runways because takeoff requires a catapult mechanism and landing uses a parachute. UAVs of this size are commonly used for tactical military missions such as target acquisition, over-the-horizon surveillance, and battle damage assessment.

Micro air vehicles (MAVs), as defined by Defense Advanced Research Programs Agency (DARPA), are miniature aircraft with a maximum wing span of 15 cm [7]. Currently, the MAV's mission is restricted by payload capabilities such as autopilot, high

resolution camera, and battery capacity. But its size benefit has the potential to overcome the UAV's accessibility in the confined area. Recently developed MAVs by the University of Florida have an 11cm wingspan and 15 minute endurance, and weigh less than 40g [8]. The University of Florida has also developed a 15cm wingspan MAV with a reconnaissance capability within 1km range with video transmitting.

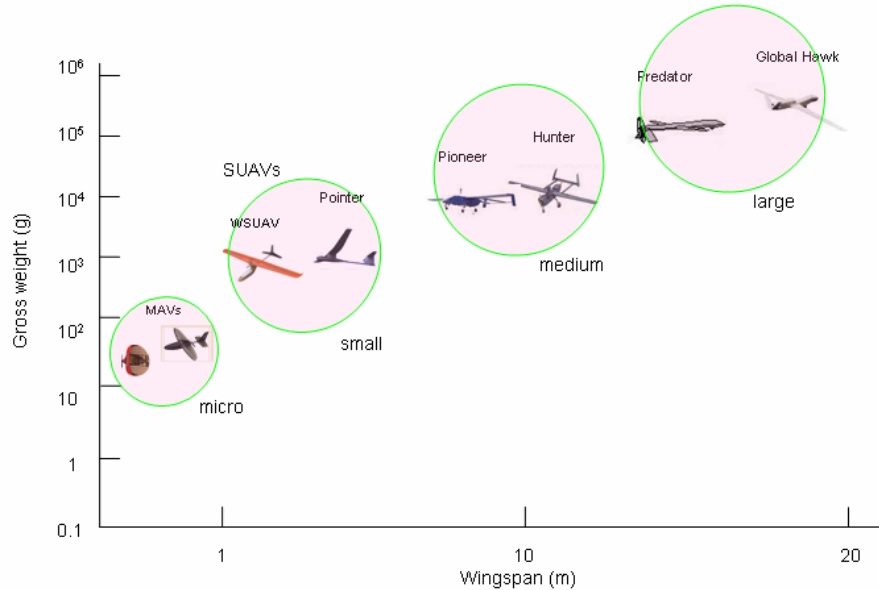


Figure 1.1 UAVs can be divided into four groups by respect to its sizes and weights.

1.2 Small Unmanned Aerial Vehicle (SUAV)

The military has shown the most recent interest in small UAVs (SUAVs) for many reasons. A SUAV is much more portable than its large counterparts and requires only one operator. A smaller reconnaissance plane can assess ground targets at a closer range without being detected. Therefore, most SUAVs use electric motors as a propulsion system, which allows for a stealthier and more reliable flight with little engine failure. Also an SUAV is less expensive and can be considered a disposable asset. This factor allows SUAV pilots to navigate hostile areas and focus on their primary mission,

rather than plane recovery. In addition to military applications, size and cost advantages are attracting civilian and private uses. Therefore, SUAVs are most suitable for use in non-military applications because they are less expensive and less dangerous. This encounter proves the need for smaller, more invisible, and more portable SUAVs.

The AeroVironment Pointer (2.7 m) SUAV was amongst the first generation of SUAVs in 1986 [9] and was designed as a tactical reconnaissance vehicle for military and law enforcement applications in confined areas. When it was released, a package of 2 airplanes and a ground station cost \$100,000. This is relatively inexpensive in comparison with mid or large size UAVs that can reach millions of dollars. The Pointer's size and reliability has already proven itself useful in Desert Storm [8]. Table 1.1 shows commercial SUAVs that are constructed by composites and are mostly designed for the military application.

Table 1.1 The wingspan and flying time of the SUAV are compared according to the manufacturer and its product.

| Name | Manufacturer | Wingspan (m) | Endurance (hr) |
|------------|---------------|--------------|----------------|
| Pointer | AeroVironment | 2.7 | 2 |
| Raven | AeroVironment | 1.28 | 1.5 |
| Dragon eye | AeroVironment | 1.14 | 1 |
| Casper-200 | Top vision | 2 | 1 |
| Skylark | El bit | 2 .0 | 1 |

1.3 Motivation of Development

Although aerial photography used for the research on wildlife habitats is advantageous, it is not always safe or easy to get quality photographs due to the many restrictions on real aircrafts.

Such restrictions include: Federal Regulation (code 14, Part 91.119): “No flying under altitudes of 305 m in populated areas” [9]. This contradicts the fact that pilots must frequently fly below 150 m in order to obtain quality photographs. The minimum practical speed is too fast for quality photographs, must meet certain criteria to operate (such as airports and weather), safety (numerous crashes), and budgeted expense. An excerpt from a report on the 2001 fiscal year from the Idaho Department of Fish and Game [10] showed that their department budget was more than \$60,000 for rental of fixed wing and rotary aircraft for surveying wildlife. Therefore, the SUAV has many advantages over their real counterparts in respect of their lower flight speed, altitude and less air-space restrictions, but a single set of commercial SUAVs generally exceed a nominal price with costs up to (\$100,000) and are usually not well suited for wildlife applications.

1.4 Thesis Objective

The purpose of this thesis is to outline the development of a reliable Wildlife surveillance UAV (WSUAV), with a wingspan less than 2m, which can be used in wildlife aerial surveys.

The discussion will focus on the overall design, fabrication and evaluation, which allow the WSUAV to be wildlife applicable. Overall, the entire WSUAV system pursues a low cost, high reliability approach to observing wildlife.

1.5 Design Metrics

In order to help guide the development of the WSUAV, a set of specification were established. The WSUAV’s performance is specified by The Florida Cooperative Fish and Wildlife Research Unit (FCFWRU).

1.6 Related Work

There are some electronic components on the market that were purchased for use in the WSUAV. The following is a list of the units:

1. Kestrel Autopilot
 - Full way point navigation
 - The Virtual cockpit software
2. Cannon Eureka progressive scan camera
3. RF link 2.4GHz video transmitter and receiver
4. AXI2028 brushless motor & motor controller
5. Futaba 9CAP Transmitter
6. RCATS Telemetry system
 - Flight data telemetry

1.7 Technical Challenge

Several significant technical challenges were overcome during the WSUAV's development.

- Robust airframe
- Parachute recovery
- High imagery video transmissions and on-board recording
- GPS way points navigation
- Amphibious capabilities
- One man operable and cartable

CHAPTER 2 WSUAV REQUIREMENTS

2.1 Mission Profile and overview

Oscillating path survey (Figure2.1) and Random path surveys (Figure2.2) have been widely used extensively by real aircraft or limited number of UAVs to estimate trends in animal populations. The use of the Oscillating path survey methods in estimating animal population size and trend can be statistically compared to pre- and post-restoration indices of species abundance. Oscillating path survey methods are likely to be successful in the near shore waters, and island regions [10] that contain shorter flight line and less bank movements. Also, these methods allow both extended flight durations and surveying areas, due to increased aerodynamic efficiency.



Figure 2.1 Oscillating path survey



Figure 2.2 Random path survey

The desired cruise speed of 22 m/s with maximum endurance of 0.5 hr and the altitude of D_1 , 150 m, from the given requirements allows for surveying about 6.3 km^2 area with 60° camera view angle as shown in Figure 2.3. The field of view and surveying area are obtained from:

$$D_2 = 2 \cdot D_1 \cdot \tan \frac{A}{2} \quad (2.1)$$

$$S_{\text{svy}} = D_2 \cdot V \cdot t_{\text{dur}} \quad (2.2)$$

Where D_1 is the altitude (m), A is the camera angle of view (θ) that describes the field of view, $D_2 \cdot V$ is the flight speed (m/s), t_{dur} is the maximum flight duration (sec), and S_{svy} is the surveyed area (m^2), as referenced in Figure 2.3

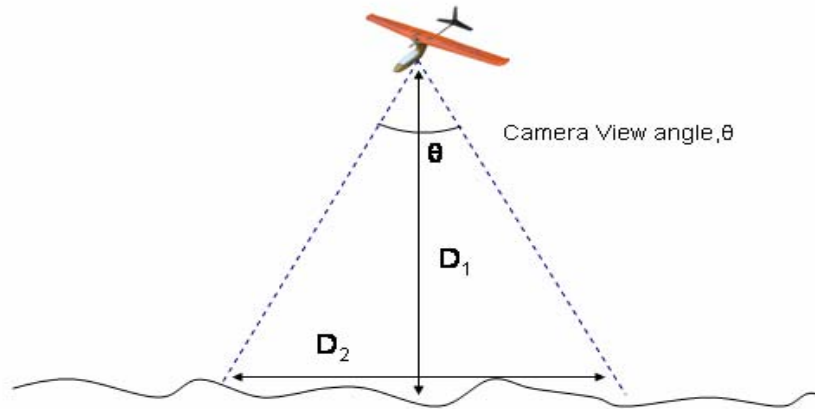


Figure 2.3 Diagram used to calculate the field of view of a camera view angle

The mission profile seen in Figure 2.4 shows a typical flight sequence for the WSUAV. The cruising sequence is 90% of the complete mission profile.

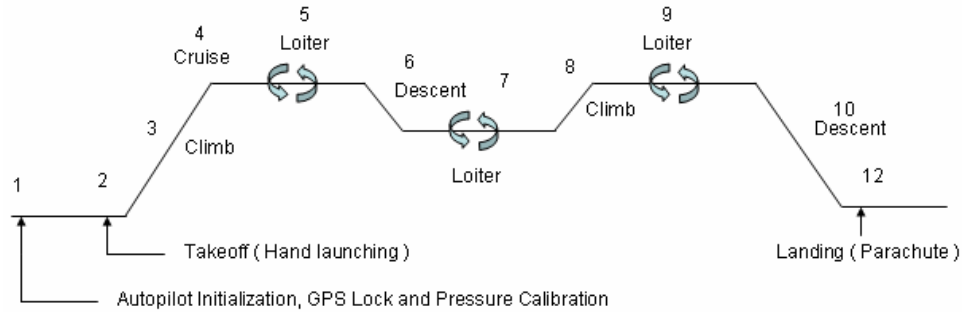


Figure 2.4 Typical WSUAV's mission profile

2.2 Design Requirements

The Florida Cooperative Fish and Wildlife Research Unit (FCFWRU) defines a WSUAV as any aircraft that meets the requirements seen in Table 2.1 below.

Table 2.1 Design requirements

| | |
|-----------------------------|-------------------------------------------------------------------------------------------------------------------------------------------------------------------------------------------------------------------------|
| Endurance | 30 min |
| Navigation | GPS / autopilot |
| Payloads | interchangeable CCD cameras, on board recording device, and sensors |
| Data transmission range | 5-10 km |
| Cruise speed and climb rate | cruise speed 80 km/h climb rate 2 m/s |
| Take-off and landing | increase hand-lunching success with less danger, Short field landings (parachute recovery), water landerable |
| Wing span | maximum 2 m |
| Propulsion | electric motor |
| Airframe | robust construction, easy repairable, inexpensive manufacturing cost, less radio communication interference due to airframe structure, major parts separately replaced (modular changeability), waterproof construction |
| Camera system | flight stability (for camera stabilization and unskilled pilots), camera lens in a safer location |
| Operation | one man operable |
| Mission altitude | 150 m from the sea level |

Table 2.2 shows the salient differences between the WSUAV and a standard SUV, including design constraints and mission objectives.

Table 2.2 WSUAV design objectives and constraints comparing SUV

| Type | WSUAV | SUV |
|-------------------------------------------------|--------------------------------------------------------------------------------|------------------------------------------------------------------------------------------------|
| Dominant design criteria | Economics and usability | Mission accomplishment and survivability |
| Performance | Maximum economic cruise GPS way points navigation | Adequate range and response GPS way points navigation |
| Take off and landing | Hand launching Parachute recovery or short landing distance, | Hand launching or launcher Adequate space for landing |
| System complexity and mechanical design | Low maintenance-economic issue Low system cost Safety and reliability | Low maintenance- availability issue Acceptable system cost Reliability and survivability |
| Government regulations and community acceptance | Low noise desirable Safety oriented Must be certifiable (FAA regulation) | Low noise desirable Performance and safety Reliability oriented Military standards |

CHAPTER 3 DESIGN OF WSUAV

3.1 Consideration to Wildlife Application and Design

Most SUAVs can be used for wildlife surveillance missions, but the design of the WSUAV is geared more towards unskilled navigators in various wildlife applications. Previous test flights exposed many problems with commercial SUAVs over Tampa Bay and select Florida wildlife recreational areas [11]. Such problems include: difficulties in finding suitable spaces for takeoff and landing, safety in hand-launching, requirements for multiple operators in the system's operation, the loss of expensive electronics by crashing into the water, and gas propulsion system failure. In particular, many SUAVs with gas propulsion systems exhibit a wide range of problems. Examples include: exhaust fouling the airframe and camera lens, engine ignition, low reliability in small size engines due to flaming out, and pronounced vibrations issues. Therefore, most SUAV manufacturers pursue electric propulsion systems. Reported problems and FCFWRU defined goals should be considered in the conceptual designing of WSUAV.

3.2 Design Process

Figure 3.1 displays the typical flow chart that governs the overall WSUAV design process. Aircraft performance and mission requirements, among others, needs to be heavily considered in the conceptual and preliminary design process. From this result, the prototype aircraft can be tested. Modification can be implemented to improve overall performance. The optimized design can lead to avionic systems, such as autopilot and video systems.

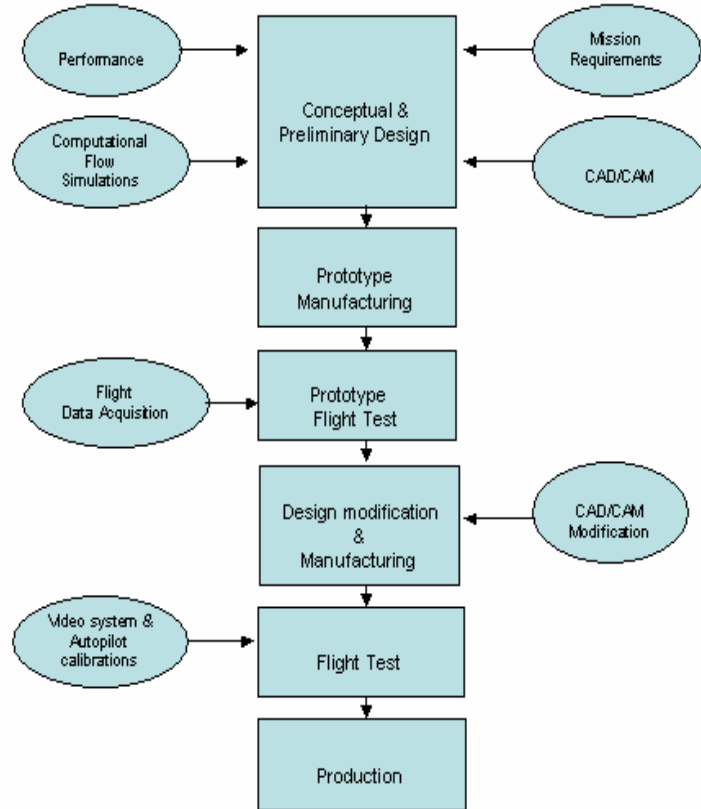


Figure 3.1 Design and manufacturing process.

3.3 Wing Design

3.3.1 Plan Form Design

The wing plan form design is considered similar to an elliptical shape, which has a high aspect ratio (more than 8). According to the Prandtl wing theory [12], an elliptical shape is ideal for minimizing drag due to lift and reducing stall speed, but it is difficult to construct. Figure 3.1 shows the lift distribution along the half wingspan. Also Figure 3.2 illustrates C_L vs Angle of Attack (AOA), which shows selected AR, 8.55, producing high lift close to infinite wing. Hence, WSUAV's wing plan form is designed as following: a taper ratio of 0.623, a high aspect ratio of 8.55, and straight leading and trailing edges similar to the elliptical platform shown in Figure 3.2. This shape increases performance

factors such as Oswald wing efficiency factor (e) and lift over drag coefficient (L/D) [12].

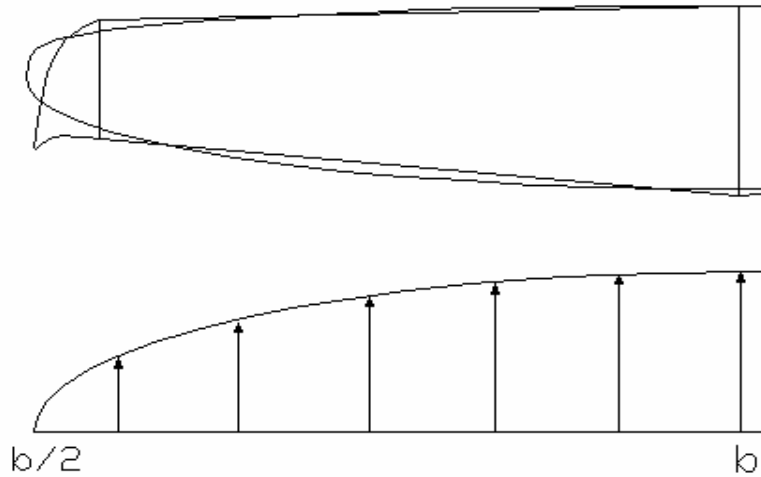


Figure 3.2 Elliptical wing platform shape comparison

Figure 3.3 shows the relative efficiencies of the theoretical aspect ratio of infinite and WSUAV plan form.

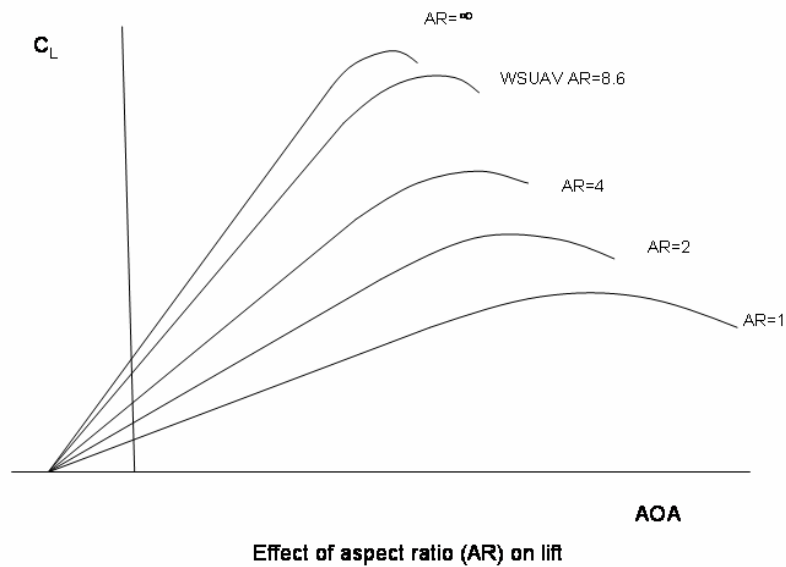


Figure 3.3 Typical effect of aspect ratio on lift

Oswald Efficiency Factor

The Oswald efficiency factor (e) is a parameter, which expresses the total variation of drag with lift [12]. It would be 1.0 for an elliptically loaded wing with no lift-dependent viscous drag. We can obtain an Oswald efficiency factor, 0.8, from the following equation:

$$e = 1.78(1 - 0.045AR^{0.68}) - 0.64 \quad (3.1)$$

Where $AR=8.55$, and leading edge sweep angle (Λ_{LE}) smaller than 30°

3.3.2 Wing Area and Airfoil Estimation

Wing area can be obtained by deciding wing loading (W/S) with other SUAV's trend values as shown in Table 3.1 [13]. Where W is the total weight of the airplane and S is a wing area. W/S is assumed to be 70 kg/ms^2 . WSUAV's W is shown in Table 3.2. $C_{L_{\max}}$ is obtained from defined stall speed at sea level [16] and V_{stall} is assumed to be 8.89 m/s .

$$V_{\text{stall}} = \sqrt{\frac{2W}{\rho C_{L_{\max}} S}} \quad (3.2)$$

Thus airfoil can be decided from $C_{L_{\max}}$ at Reynolds number (Re) of 385,970. Re is given as:

$$Re = \frac{\rho \cdot V \cdot L}{\mu} \quad (3.3)$$

Where L is mean chord length from wing plan form, 0.25, and V is 22 m/s at sea level.

Table 3.1 WSUAV weight distribution, $W (3.371 \text{ kg}) = W_{\text{empty}} + W_{\text{avionics}} + W_{\text{battery}} + W_{\text{propulsion}}$. It shows all components and weights for WSUAV.

| | | Part name | Weight (g) |
|-----------|----|--------------------------|------------|
| Structure | 1 | Fuselage | 260 |
| | 2 | AXI motor | 155 |
| | 3 | Controller | 48.1 |
| | 4 | Wing (right) | 400 |
| | 5 | Wing (left) | 400 |
| | 6 | Wing connector | 60 |
| | 7 | Elevator servo | 25 |
| | 8 | Aileron servo (flat) | 30 |
| | 9 | Wing screw | 6.8 |
| | 10 | Thunder power(4s4p) | 645 |
| | 11 | Propeller | 19.3 |
| | 12 | Propeller hub | 17.5 |
| | 13 | Stabilizer unit | 187 |
| | 14 | Tail pipe | 53 |
| | 15 | Hatch | 70 |
| | 16 | Protective foam | 35 |
| | 17 | Computer case | 70.5 |
| | 18 | Pitot tube | 10 |
| | 19 | Bulkhead | 17 |
| | 20 | CA glue | 20 |
| | 21 | Parachute | 176 |
| | 22 | Parachute deploy device | 10 |
| Avionics | 1 | Kestrel autopilot | 55 |
| | 2 | Furuno GPS | 18 |
| | 3 | 500 line CCD camera | 61 |
| | 4 | 380 line CCD camera | 30.5 |
| | 5 | Aerocomm modem | 20 |
| | 6 | Modem antenna | 9 |
| | 7 | 6v regulator | 19 |
| | 8 | Autopilot wire bundle | 8 |
| | 9 | Camera switching device | 9 |
| | 10 | 1200mA autopilot battery | 74 |
| | 11 | 250mW Video transmitter | 19.3 |
| | 12 | Canon recorder | 300 |
| | 13 | Video overlay device | 33 |
| | | Total weight (W) | 3371g |

The airfoil should be designed to correspond to $C_{L_{max}}$ and Re estimated above.

Also other wing loadings under cruise flight conditions are obtained from following equation, and then compared with the assumed wing loading, 70 kg/ ms^2 . Cruise condition which the lift equals the wing loading divided by the dynamic pressure where ρ is air density at the sea level as shown in Equation 3.4.

$$\left(\frac{W}{S} \right)_{\text{cruise}} = \frac{1}{2} \cdot \rho \cdot V^2 \cdot C_L \quad (3.4)$$

Table 3.2 shows other SUAV's wing loadings.

Table 3.2 W/S comparison with other SUAVs [13]

| Name | PSUAV | Casper | WSUAV |
|------------------------|-------|--------|-------|
| W/S, kg/ ms^2 | 65.9 | 70.8 | 70 |

3.3.3 Airfoil Design

The airfoil is the essence of the airplane, which affects the take off, landing, cruising, and stall speed. Also, its maximum aerodynamic efficiency and L/D at a defined cruising speed will increase the duration of the flight. The WSUAV's airfoil design should be more focused on the cruising condition than other flight phases, such as take off and landing. This is because mission requirements show that the cruising condition is nearly 90% of total flight time. Many institutes such as NACA, Eppler, Selig, etc, have designed and tested laminar flow airfoils at various Reynolds numbers to achieve a higher lift to drag ratio. Most developed airfoils are designed for high speed or in a high Reynolds region (more than 1 million), but most SUAVs are operate in a Reynolds number region under 500,000. Many Selig airfoils, in particular, are designed for the low

speed application. Sometimes existing airfoils are suitable for the small aircraft applications, but modifications or new designs are preferred for acceptable off-design performance. The airfoil NACA 2411 [14] is chosen for the initial model in order to meet $C_{L_{max}}$ required for the stall speed at estimated Re .

Design Method

The direct design method is used in the XFOIL interactive program, which involves specification of section geometry and calculation of pressures and performance. We evaluate the given shape and then modify the shape to improve the performance. XFOIL is an interactive program for the design and analysis of 2D subsonic isolated airfoils with varied Reynolds numbers. The plotted geometry, pressure distribution, and multiple polar graphs were used for calculating lift and drag at varying angle of attack, their results are depicted in the following Figure 3.5, 3.6, 3.7, and 3.8. Figure 3.4 shows the LKH 2411 Airfoil, which is created through the XFOIL program, based on NACA 2411 airfoil specifications for creating a higher lift to drag ratio, and less pitching moment coefficient at maximum L/D as shown in Figure 3.8. The following Figure 3.4 shows this airfoil shape, which has a maximum of 11% thickness. Maximum camber is located at 40% of chord. Also, the coordinate of airfoil can be found in Appendix A. Figures 3.5 through 3.8 shows the simulated results from the XFOIL program at Re of 385,970. In Figure 3.7, the ratio of the lift and drag coefficients for the airfoil show a substantial improvement over the NACA 2411. The comparison data can be found in Appendix B. While the credibility of this result is under suspicion, the comparison can still serve as a reasonable design base. From these results, we can use this data for the aircraft wing design.

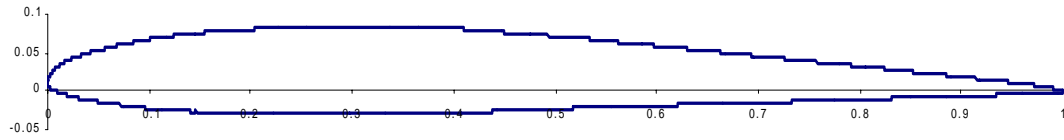
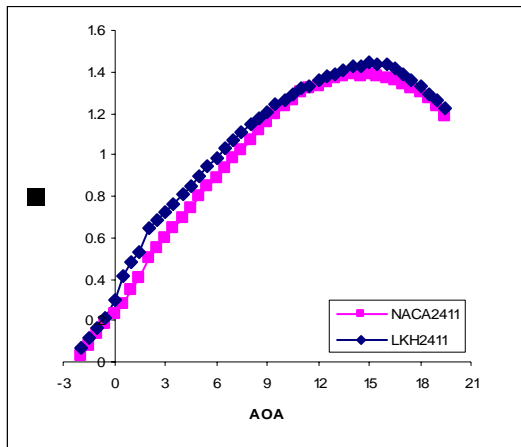
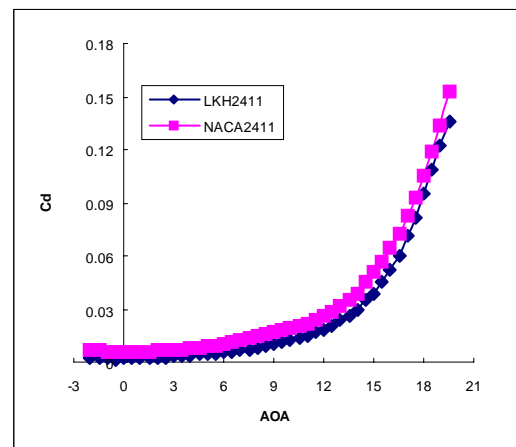
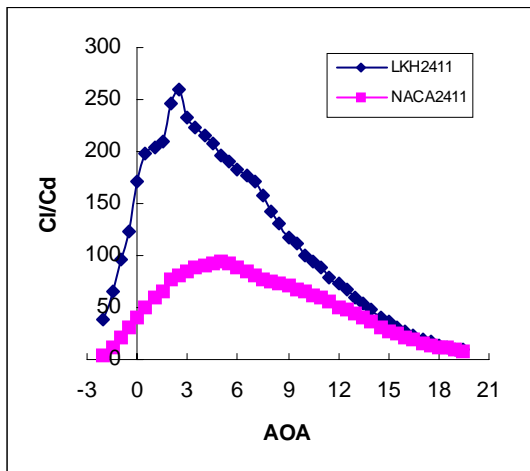
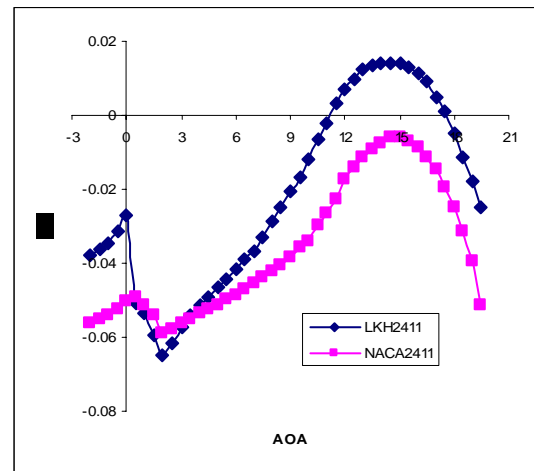


Figure 3.4 LKH 2411 airfoil at 2.5° AOA

Figure 3.5 C_l vs AOA for LKH 2411 & NACA 2411Figure 3.6 C_d vs AOA for LKH 2411 & NACA2411Figure 3.7 C_l/C_d vs AOA for LKH 2411 & NACA 2411Figure 3.8 C_m vs AOA for LKH 2411 & NACA 2411

3.3.4 Aerodynamic Calculation

Weight, Lift and Drag at Cruise

The cruise flight parameters of lift and drag at a cruise condition may be calculated according to 3.2. In a cruise flight condition weight should equal lift and drag should equal thrust.

$$L_{\text{cruise}} = \frac{1}{2} \cdot \rho \cdot V^2 \cdot C_L \cdot S \quad (3.5)$$

$$D_{\text{cruise}} = \frac{1}{2} \cdot \rho \cdot V^2 \cdot C_D \cdot S \quad (3.6)$$

Takeoff, Landing Speed and T/W

Given a $C_{L\text{max}}$ value for a wing as found in Figure 3.7 the stall speed of the aircraft may be calculated in Equation 3.3. Based on Raymer's historical data [12] the landing and takeoff speeds may be estimated from the stall speed. From this the takeoff and landing lift and drag coefficients may then be calculated.

$$V_{\text{landing}} = V_{\text{stall}} \cdot 1.2$$

$$V_{\text{takeoff}} = V_{\text{stall}} \cdot 1.4$$

$$C_{L_{\text{takeoff}}} = C_{L\text{max}} \left(\frac{V_{\text{stall}}}{V_{\text{takeoff}}} \right)^2 \quad (3.7)$$

The T/W ratio is best chosen based on similar aircraft. Table 3.3 indicates the T/W ratio of two other similar SUAV's and the selected value of T/W for the WSUAV.

Table 3.3 T/W comparison with other SUAV

| Name | Pointer SUAV | Casper-200 | WSUAV |
|------|--------------|------------|-------|
| T/W | 0.5 | 0.47 | 0.48 |

Take Off Parameter (TOP)

Equation 3.6 may be used to calculate the takeoff parameter which is an indication of an aircraft's basic takeoff performance. For an airplane such as the WSUAV a TOP, 228, greater than 200 would be sufficient for a hand-launch takeoff [12].

$$TOP = \frac{(W/S)}{\sigma \cdot C_{L_{takeoff}} \cdot (T/W)} \quad (3.8)$$

Where σ is a air density ratio = air density at takeoff / sea level

Parasite Drag, C_{DO}

Equivalent Skin-Friction Method for the estimation of the parasite drag, C_{DO} , as shown in Equation 3.7 is used for obtaining of a skin friction-drag and small separation pressure drag. Equivalent skin friction coefficient, C_{fe} is a 0.003 for the smooth surface composite of the airplane [12]. Reference area, S_{ref} , and Wetted area, S_{wet} , are calculated through the ProEngineer 3D drawings. As shown in Figure 3.6 which depicts the simulation result, C_l equals 0 at -2.6° AOA and C_{DO} is 0.01. The two values show a difference of only 0.0067. Hence, we can assume a reasonable value of C_{DO} .

$$C_{DO} = C_{fe} \cdot \frac{S_{wet}}{S_{ref}} \quad (3.9)$$

Where S_{wet} is 3.86 and S_{ref} is 0.685.

Induced Drag (Oswald Span Efficiency Method), C_{Di}

Induced drag due to nonelliptical lift distribution and flow separation can be accounted for using the “Oswald efficiency factor”, which is dependent upon AR ratio. K is obtained at following Equation 3.10 [15]. The Induced Drag, C_{Di} is obtained from following Equation 3.11.

$$K = \frac{1}{\pi \cdot e \cdot AR} \quad (3.10)$$

$$C_{Di} = K \cdot (C_L - C_{L \text{ min drag}})^2 \quad (3.11)$$

A C_L value of 0.6 and a $C_{L \text{ min drag}}$ value of 0.1 are obtained from Figure 3.9 below.

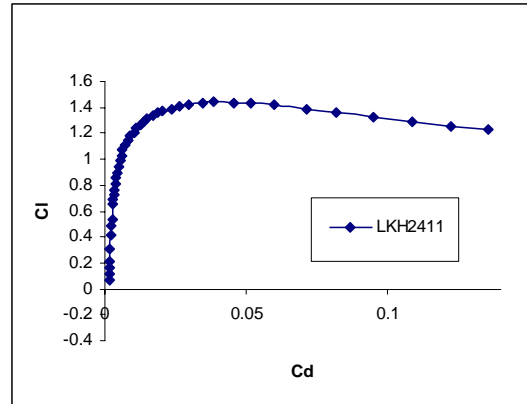


Figure 3.9 LKH 2411 C_l vs C_d

Maximum Ceiling

The Maximum Ceiling, 8700 m, is obtained from p in the Standard Atmosphere chart [15] at given velocity, V , and selected wing loading, W/S (70 kg/ ms^2) using Equation 3.12.

$$\frac{W}{S} = q \sqrt{\pi \cdot e \cdot AR \cdot C_{Do}} \quad (3.12)$$

$$\rho = \frac{2 \cdot W/S}{C_L \cdot V^2} \quad (3.13)$$

Where q is $(1/2) \cdot \rho \cdot V^2$.

3.3.5 Computational Fluid Dynamics (CFD) Simulation

Computational Fluid Dynamics is the process of solving the incompressible 3D Navier-Stokes equations on a certain object by using a pressure-based algorithm [16]. CFD is the practical solution to a complicated problem involving the WSUAV. The Reynolds Number of the WSUAV is computed to be around 400,000. This number is computed using the dimensions of the WSUAV wing. For the WSUAV wing to be scaled down properly (under 50 cm) for use in the University of Florida's wind tunnel, the wind speed must be increased fourfold, which is unobtainable due to lack of facilities. Three wing designs (Figure 3.10) of the same airfoil (original design created by using X-Foil software) were tested to determine the most efficient shape. The three plan form designs that were tested are shown in Figure 3.10 below. All tested designs have the same overall wing area. Design one used a winglet-less concept. Design two and three incorporated winglets. Design two used a 20 degree dihedral curved leading edge winglet while design three used a straight leading edge 30 degree dihedral winglet.

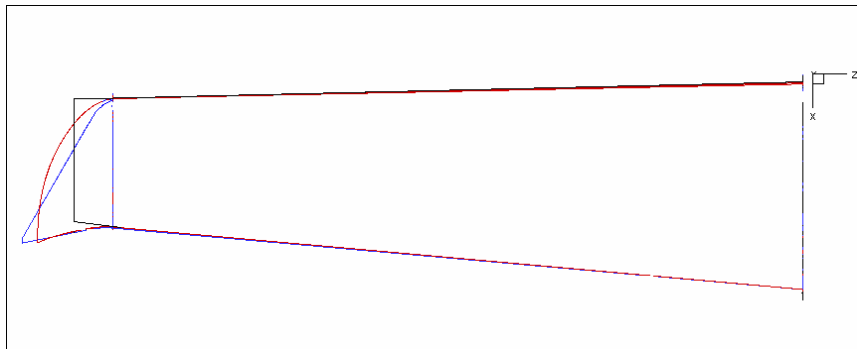


Figure 3.10 Tested wing platforms comparison

The most efficient flight and cruise is generally achieved by the use of smooth, streamlined shapes that avoid flow separation and minimize viscous effects. Figures 3.11 through 3.16 show the pressure distributions over the wing, as well as provide a visual of the airflow such as tip and wing rear side vortexes during a simulation of maximum C_L/C_D flight condition. The color Keyes describes pressure distributions in Pascals.

Simulation conditions are as follows:

- AOA = 2.5° (maximum C_L/C_D condition from Figure 3.6)
- Free stream velocity (U) = 25 m/s (maximum flight speed)
- Stream air density and viscosity = 1.225 kg/m^3 , $1.79 \times 10^{-5} \text{ kg/ms}$

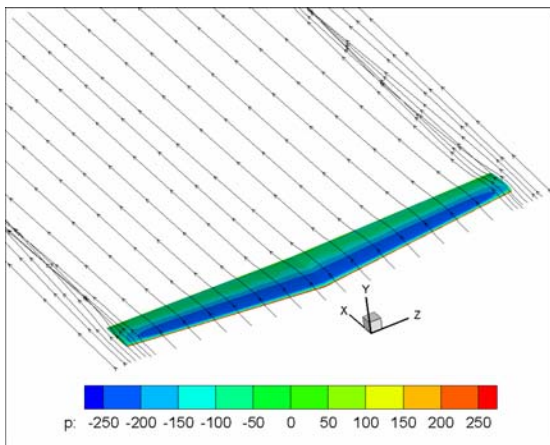


Figure3.11 CFD simulation for design one

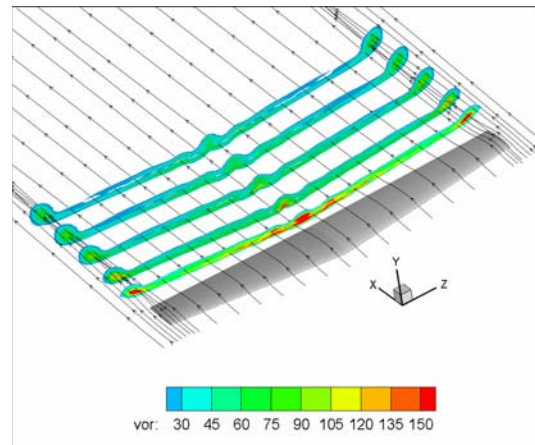


Figure3.12 Vorticity simulation for design one

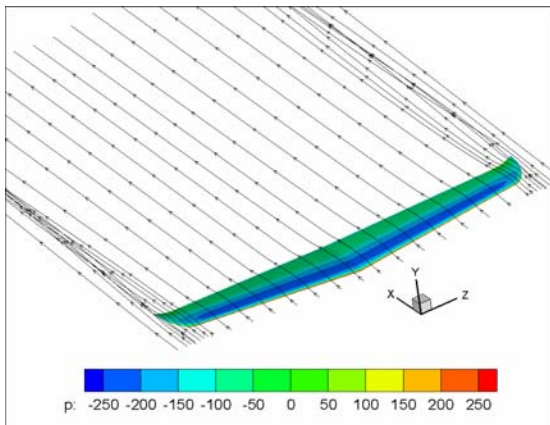


Figure3.13 CFD simulation for design two

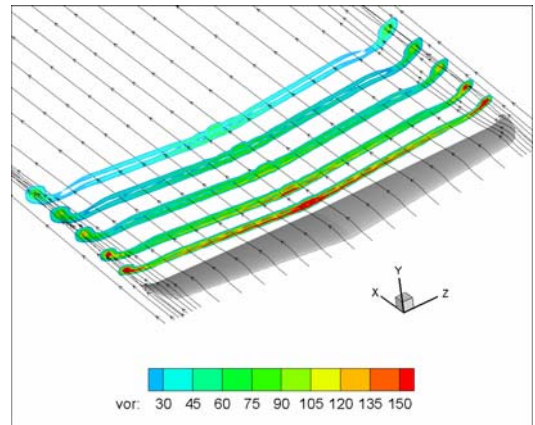


Figure3.14 Vorticity simulation for design two

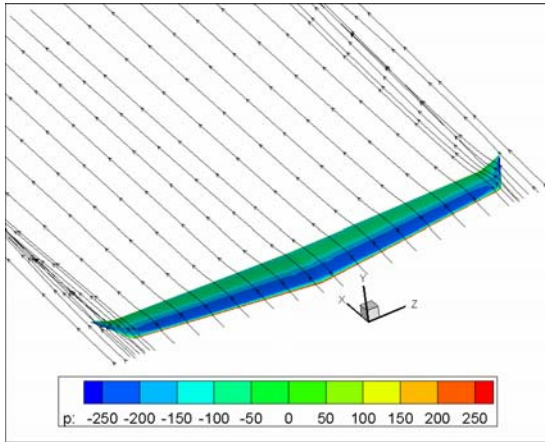


Figure3.15 CFD simulation for design three

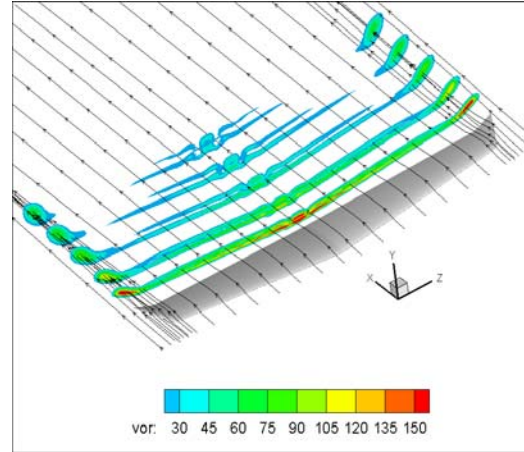


Figure3.16 Vorticity simulation for design three

Table 3.4 displays the relevant results mined from the CFD computations. τ_x and τ_y are the corresponding shear stresses over the wing. The lift to drag ratio is the most critical factor in aircraft design and performance.

Table 3.4 CFD flows and pressure visualizations results comparison

| Case | Total Lift [N] | Total Drag [N] | τ_x [N] | τ_y [N] | Lift / Drag |
|----------|----------------|----------------|--------------|--------------|-------------|
| Design 1 | 49.040 | 4.855 | 0.713 | 0.046 | 10.099 |
| Design 2 | 57.179 | 4.910 | 0.653 | 0.054 | 11.646 |
| Design 3 | 57.515 | 5.343 | 0.674 | 0.046 | 10.764 |

From the simulated results as shown in Table 3.4, we can obtain more accurate C_L and C_D values. Table 3.4 shows Design 2 produces the highest lift and L/D. Therefore, this model can be selected for the WSUAV's wing model.

3.3.6 Wing Dihedral

The purpose of dihedral is to improve lateral stability that has correlation with the pendulum effect (center of gravity location in vertical axis) and wing sweep angle. If a disturbance causes one wing to drop, the unbalanced lift forces produce a sideslip in the direction of the down going wing because of its higher drag. This will, in effect, cause a

flow of air in the opposite direction to the slip. At the moment, lower wing produces more lift than upper wing with dihedral and the airplane will roll back into neutral position. WSUAV's lateral stability is expected simply well because its wings are attached in a high position on the fuselage which contains most payloads. When the airplane is laterally disturbed and as a result one wing moves down, this payload acts as a pendulum returning the airplane to its original attitude. Therefore a 2° dihedral angle is considered following trend value for an upswept, high wing [15] for the design to assist lateral stability.

Designed Wing Specifications:

Span = 2 m

Span without angled tip = 1.83 m

Area, S: main wing (0.443m^2) + tip (0.027 m^2) = 0.47 m^2

Aspect Ratio, $AR = b^2/S_{\text{ref}} = 2^2/0.47 = 8.55$

Taper Ratio, λ , $C_{\text{tip}}/C_{\text{root}} = 0.187/0.300 = 0.623$

Mean chord length, $C_{\text{mean}} = 0.243$

Sweep Angle, $\Lambda_{C/4} = 0^\circ$

Leading Edge Sweep Angle, $\Lambda_{\text{LE}} = 1^\circ$

Wing dihedral = 2°

Tip dihedral = 25°

Aerodynamic Center location, AC = 0.1m from Leading Edge

Maximum thickness of airfoil = 11% of chord

Maximum camber location of airfoil = 40% from the leading edge

The final design model is drawn with ProEngineer 3D design software for the CNC manufacturing and future modifications, as shown in Figure 3.17.

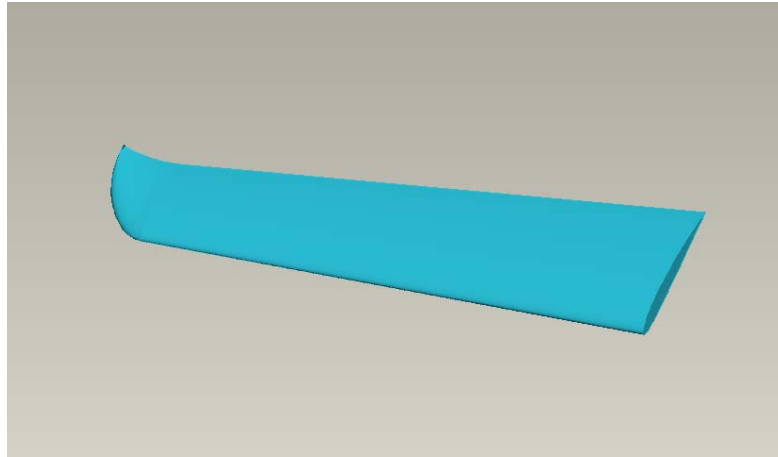


Figure 3.17 The final design of the right wing

3.4 Fuselage Design

The fuselage design can be divided into three different respects; structure, payload distribution (CG consideration), and aerodynamics.

3.4.1 Structural Considerations

Major components are attached and contained in the fuselage. Many stresses are applied to the fuselage: wing lift and drag through the four mount bolts, stress from the stabilizers through the tail boom, thrust from the motor, and landing impact. Therefore, the fuselage needs to be robust in construction in order to handle applied stresses from demanding flying conditions, hard landings, and minor damages. WSUAV's were specifically designed without landing gear in order to reduce overall weight and drag, but also to decrease the stress absorbed by the fuselage at the connection spot of the landing gear. Another reason the fuselage needs to be sturdy is because it contains fragile avionics such as the following: autopilot, GPS, modem, video recorder, two cameras, video transmitter and antennas. The fuselage of WSUAVs are fabricated with non-

interfering radio wave materials so that antennas can be installed and protected in the fuselage. The configuration of internal antennas can make smoother fuselage surface and in-turn reduce drag and damage to the antenna

3.4.2 Consideration of Center of Gravity (CG)

The payload's distribution in the fuselage mainly affects two CG positions, one along the fuselage and the other along the vertical axis. The CG position along the fuselage axis is very important in achieving longitudinal stability. Its distance from the Aerodynamic Center (AC) point of the airplane is called Static Margin (SM) which affects the longitudinal stability. For stable flight, the CG is usually placed before the AC, and payloads that are placed too far behind the CG the result is a tail-heavy airplane with smaller or negative SM. It results in nose-up attitude which causes difficulties in control of the airplane in the longitudinal because of its higher sensitivity.

The CG position along the vertical axis is very important in achieving lateral stability. WSUAV has a longer distance between CG and AC points in the vertical axis than other SUAVs because location of the propulsion system requires propeller tip clearance. See Figure 3.18. This factor creates a great advantage in achieving more Lateral stability. Therefore, the CG position should be determined in relation to the heavier components' location and distribution in the fuselage. Once the CG position of the WSUAV is fixed, it will be invariable because the weight of the main battery in the propulsion system is constant (Figure 3.18).

The moment estimation method used is detailed below, using component weights adopted from Table 3.2. For estimating the center of gravity, each payload moment arm is multiplied by its weight. This CG position should be in front of the AC position for a

$$C_{Di} = \frac{C_L^2}{s \cdot e \cdot \pi \cdot AR} \quad (3.14)$$

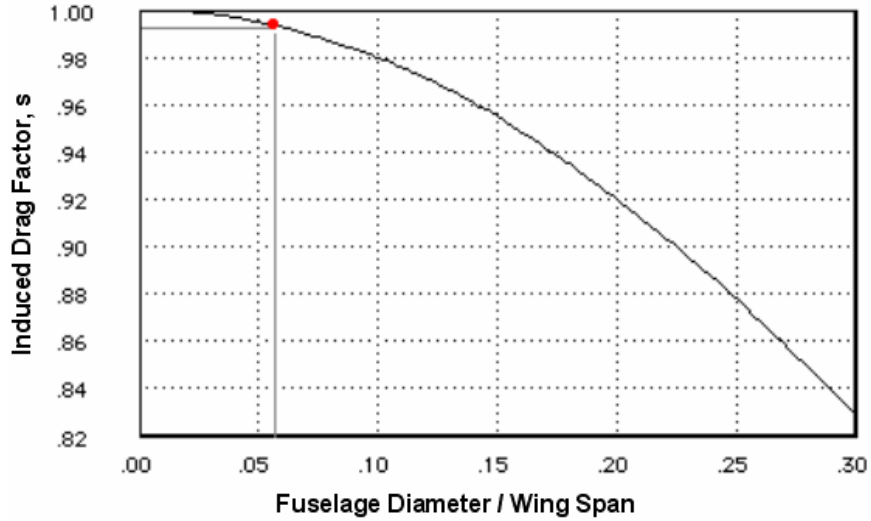


Figure 3.19 Lift-dependent factor for fuselage interface [17]

3.4.4 Consideration of Hatch Design

The hatch is another important part of the fuselage. During field operation, accessibility is crucial to the changing of batteries, adjustment of camera angles, and the maintenance of avionics. Watertight hatches should be considered for WSUAV to minimize electrical damage during parachute landing on the water. The size of the battery and other electric components should determine the size and location of the access hole.

3.5 Stabilizer Design

The airplane's performance, especially in longitudinal and lateral-directional stabilities and controls, is affected by the stabilizer's design, for example, its size, shape and location. If the stabilizer is too large in size, it will cause high restoring forces and also increase the airplane's drag. Eventually, the aircraft will oscillate with higher

amplitude until it goes out of control. Inversely, smaller size stabilizers create statically unstable conditions that cause the plane to stall at higher speeds. However, static stability is opposite to dynamic stability. If design requirements do not pursue agility or maneuverability, and since a WSUAV'S mission requirements consist of basic loiters and turns. In the case of dynamic stability, it means the airplane will return to its original condition by restoring or damping forces [18]. This characteristic will help to collect more stable video imagery along with important data from the airplane's operation. This is especially useful in the hands of unskilled pilots. Even though high levels of calculation have been done, the final design and placement of the stabilizer should be corrected through many test flights. Three different shapes of stabilizers were tested by test flights as shown in Figure 3.20. Also Table 3.5 shows its specifications. From test flights with an anhedral type stabilizer, it has been shown that airplane landings in tall weed areas could have a damaging affect to the airplane. The horizontal stabilizer with an anhedral configuration is easily damaged by weeds. Therefore, it is better to select the stabilizer with a conventional shape or 'V –Shape' configuration. The previous test flights with the "V-shape" exhibited coupling, pitching, yawing, and problems. In the conventional design, it showed that the effectiveness of the vertical stabilizer because of less interference with the propeller slip stream [19]. Due to these factors, the conventional configuration in Figure 3.20 was selected as the final design. The airfoil used for the tail in each configuration is the EH0.0/9.0 and its coordinates can be found in Appendix C.

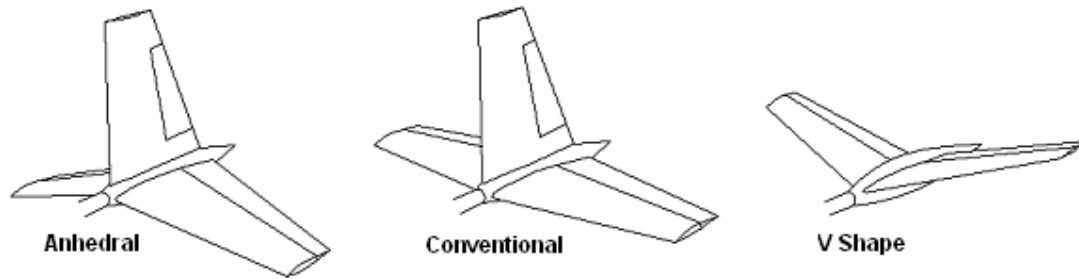


Figure 3.20 Tested stabilizer configurations

Table 3.5 shows the difference between the angles seen in the three configurations. λ is the aspect ratio, and Λ_{LE} is the leading edge angle.

Table 3.5 Tested stabilizer specifications

| Shape | Projected S_{HT}, m^2 | Projected S_{VT}, m^2 | Angle between S_{HTA} and S_{VT} , Degree | Airfoil | λ | Λ_{LE} , Degree |
|--------------|-------------------------|-------------------------|-----------------------------------------------|-----------|-----------|-------------------------|
| Anhedral | 0.072 | 0.038 | 100 | EH0.0/9.0 | 0.5 | 8 |
| Conventional | 0.0767 | 0.044 | 90 | EH0.0/9.0 | 0.5 | 8 |
| V-Shape | 0.07 | 0.07 | 120 | EH0.0/9.0 | 0.5 | 8 |

Tail Volume Coefficient, C_{VT}, C_{HT}

Tail moment and tail area are not independent items. For a given amount of pitch or yaw stability, there is a linear relationship between static stability and either tail area or tail moment.

Vertical and Horizontal tail volume coefficient, C_{VT} and C_H , are used for the estimation of tail size. These numbers show how strongly tail is to counter moments generated by the wing. In other way, tail size is proportionally related wing size. From the results in the following equations, C_{VT} and C_{HT} values of 0.0368 and 0.534 are selected to satisfy the trend [12].

$$C_{VT} = \frac{L_{VT} \cdot S_{VT}}{b_w \cdot S_w} \quad (3.15)$$

$$C_{HT} = \frac{L_{HT} \cdot S_{HT}}{C_w \cdot S_w} \quad (3.16)$$

Where S_w is wing area, S_{VT} is vertical tail area, S_{HT} is horizontal tail area, b_w is wing span, and C_w is mean code length.

Designed Stabilizer Specifications

Horizontal Stabilizer: $AR = b^2/S_{ref} = 0.59^2/0.0767 = 7.69$

Taper Ratio, $\lambda = 0.5$

Sweep Angle, $\Lambda_{C/4} = 4^\circ$

Area, $S_{HT} = 0.0767 \text{ m}^2$

Vertical Stabilizer: $AR = b^2/S_{ref} = 0.295^2/0.044 = 1.98$

Taper Ratio, $\lambda = C_{tip}/C_{root} = 0.103/0.196 = 0.5$

Leading Edge Sweep Angle, $\Lambda_{LE} = 8^\circ$

Sweep Angle, $\Lambda_{C/4} = 4^\circ$

Area, $S_{VT} = 0.044 \text{ m}^2$

Drawings of WSUAV

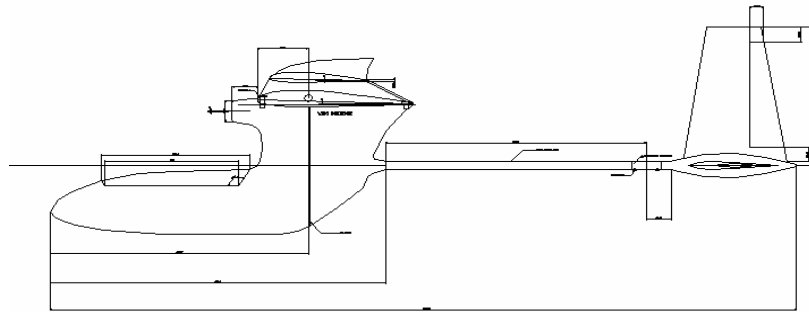


Figure 3.21 Side view

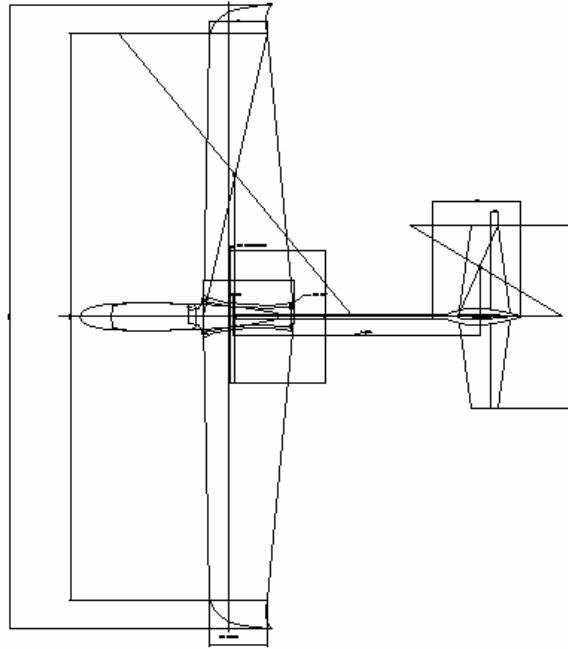


Figure 3.22 Top view

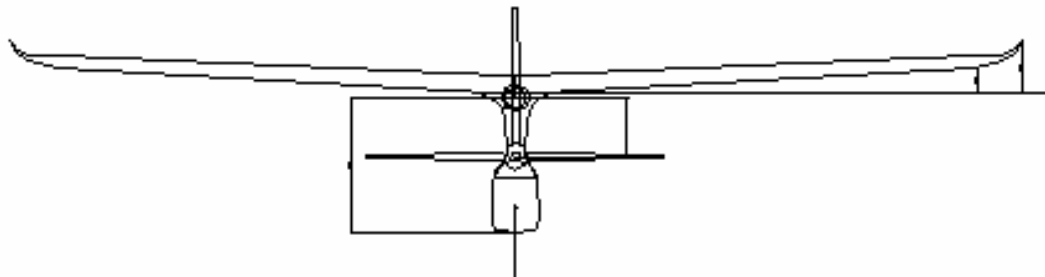


Figure 3.23 Front view

3.6 Propulsion system

The propulsion system consists of three sections; they are electric motor, propeller, and battery. Besides these three components, the aerodynamics of the airplane, such as lift over drag vs. speed, should be examined to attain true optimum conditions in the propulsion system of the aircraft. Figure 3.24 gives an illustration.

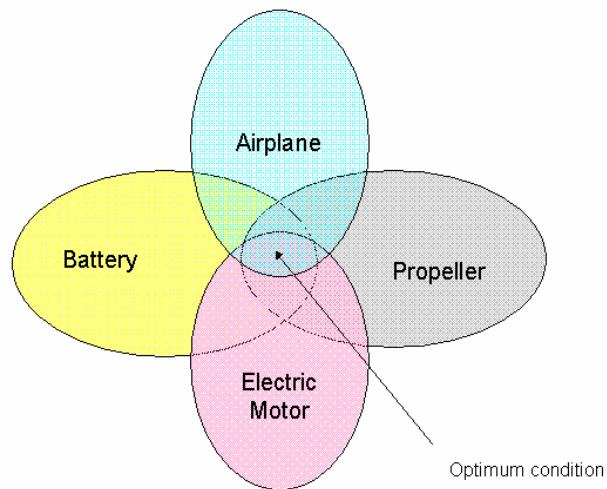


Figure 3.24 Optimum condition of propulsion system.

3.6.1 Electric Motor Selection

There are two different types of electric motors that can be used. The first type is the brush motor which has an internal contact between the brush and the armature. During high frequency switching, this contact may cause arcing and heating especially at high currents. This problem contributes to a major hindrance in its cooling. Motor cooling is directly related to establishing maximum efficiency.

The second type is the brushless motor, which generates higher torque with less heat because the effective resistance of the brushes is much higher. Foremost, brushless motors can fit much thicker wires than a brush motor of equivalent size, thus lowering resistance, increasing efficiency, and increasing torque. Because of these facts, brushless motors have the inherent capability to spin faster, operate at higher currents, and produce more power without the performance deteriorating at high currents and temperatures. Hence, most recent UAVs have been using the lighter-weight, smaller brushless type motor in order to get higher power with less radio noise generated to interfere with the

avionics. This benefit will increase the reliability of the communication between airplane and ground station.

3.6.2 Cooling Consideration

Electric motors are mounted so that they receive ample airflow through the magnets and armature. To maintain a safe operating temperature, the motor must be cooled to less than 130° C [20] or else overheating of motor will occur. Extensive heating causes increased wear in bearings and partial demagnetization. These failures will significantly decrease the performance of the motor and consequently the battery.

A recently developed rotating-case brushless motor has been designed to produce higher torque and therefore allow the use of large size propellers without gearboxes. The rotating case design was implemented for two reasons: increased cooling and torque. The case provides self-cooling because of its rotating action, thus forcing air between the magnets and armature. The rotating case dismisses the need for a gear reduction unit because in the spinning case more circular momentum is created. The specifications for the casing drive motor are shown in Table 3.6.

Table 3.6 Specifications of electric motor

| | |
|------------------------|----------------|
| Model | AXI2820/10 |
| Voltage range | 9.6-16 V |
| RPM/V | 1,100RPM/V |
| Max.Efficiency | 80% |
| Max.Efficiency Current | 15-35 A (>73%) |
| Typical trust, T | 14-18 N |
| Internal resistance | 42 mW |
| Dimensions | 35.2x54.5 mm |
| Propeller range | 10"x6"-12"x8" |

T/W from Table 3.3 is 0.48, and $W = 3.371$. We can obtain $T = 15.85$ N, which is required. From the Table 3.6, AXI 2820/10 motor has a 14-18 N thrust range. Hence, this motor is accepted for the airplane design.

3.6.3 Battery Selection

Flight duration is mainly dependent upon a battery's performance. Meaning that its better to have a lightweight battery with a high capacity under high loaded conditions, as well as having a high energy density (Wh/kg). Recently, battery technology has risen to a new level. Representative of these new higher energy density batteries are: disposable LiSO₂ (Lithium Sulphur Oxide), rechargeable LiON (Lithium Ion), and rechargeable Lithium-Polymer as shown Figure 3.25 [20]. These batteries display good discharge rates at high and low-temperatures. This new lithium technology has proven to be successful in military SUAVs with respect to duration, reliability, and cost. The outcome of this is smaller and smaller SUAVs with longer flight durations. Lithium-Polymer is the battery of choice for the WSUAV because of its high energy density and cost effective, reusable characteristics.

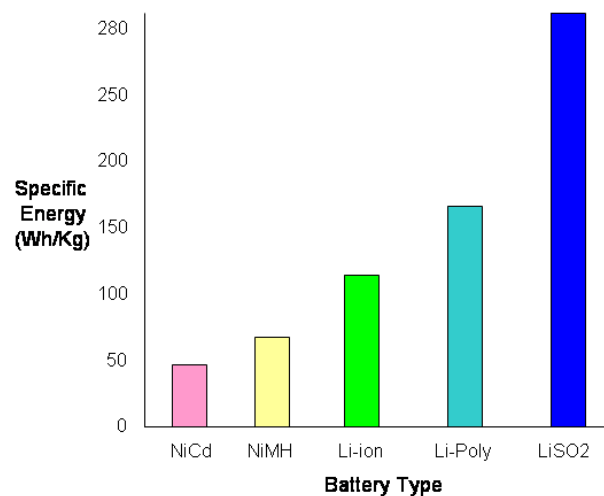


Figure 3.25 Gravimetric energy density for various batteries

Table 3.7 Specifications of selected battery

| | |
|------------------------|-------------------------------|
| Specification | Thunder power 2050 4S4P |
| Nominal Capacity | 7600mA (112.5 Wh) |
| Output | 14.8 V |
| Dimension | 50mm x 245 mm x 28 mm (616 g) |
| Applications | RC aircraft and helicopters |
| Max. Current Rating | 5C max Avg. Discharge |
| Impedance (ohm) | 0.0125 |
| Energy Density (Wh/kg) | 182.6 |

Table 3.7 shows the exhibited specifications of the selected battery. It shows a five times greater discharge rate of nominal capacity of the battery, providing constant power to the motor. The battery also has a comparably higher energy density.

Endurance Estimation

The maximum flight endurance is estimated by battery capacity (Wh), P_{bat} , and total power consumption of the propulsion system [21], P_{to} , is displayed in Table 5.1.

$$t_{mxpw} = \frac{P_{bat}}{P_{to}} \quad (3.17)$$

t_{mxpw} is the endurance at maximum power consumption.

The value of t_{mxpw} is 0.33 hr when the propulsion system consumes maximum power. At cruise, 60% power is required due to partial throttle management. The calculated value of endurance at cruise, 32.7 minutes, meets given requirements of 30 minutes.

CHAPTER 4 AIRPLANE FABRICATION

4.1 Wing Fabrication

Wing structures are exposed to torsion and bending stress in high speed conditions and subject to deformation by ultra violet rays and heat from the sun. As a result, the wing must have a large strength-to-weight ratio and considerable flexibility to handle the high forces. The wing structure in the prototype WSUAV's, made from balsa sheets (1.8mm), sandwiched between thin outer layers of Monokote (polyester film) with a foam core. The foam core is cut by a CNC foam cutter. This manufacturing method is very useful for the prototype concept, which with moderate precision can be changed to different wing shapes. Unfortunately, this kind of wing can be easily damaged by a hard landing or crash. Therefore, the final design of the wing should be manufactured completely out of composite materials, which can pursue a higher strength-to-weight ratio and define a greater consistency in its manufacturing.

Wing construction of the WSUAV requires the use of advanced composite technologies. Due to the advanced platform, certain techniques were developed allowing for a more methodical approach to the precise preparation of a suitable wing. These steps include:

Step one: (Development of the master shape)

Extensive research was done to ascertain the most suitable wing for the WSUAV application. This research yielded the LKH2411 airfoil. From this airfoil, polynomial equations of the wing surfaces were taken and certain data points were acquired. These

data points were transferred to a CNC hotwire machine which mechanically generated the LKH2411 airfoil from foam. This foam wing is the core basis for the final composite wing. In consideration of its development, the foam core was made smaller than the original shape, due to the future additions of balsa skin and fiberglass coverings. After the initial skin coverings are installed, a polyurethane paint layer is applied in order to sustain a smooth surface. This can be polished, creating a glossy finish for the female mold surfaces.



Figure 4.1 Master wing shape (right side) for the creating mold

Step Two: Creating mold

Once the master shape is completed, it will be used for the core of an epoxy gel coat mold. For releasing purposes, multiple layers of Frekote releasing agent are applied to the surface of the master shape. Once the releasing agent is applied, an epoxy gel coat mixture is created and poured over the master shape, but before this can be done, the master shape must be divided in two by creating a dividing surface along the centerline. After the gel coat is applied and before it dries, multiple layers of unidirectional

fiberglass weave and epoxy are added to gain strength for the mold structure. Allowing the gel coat and epoxy to dry, the newly formed half side of the mold is removed and the same process is done for the remaining side. Figure 4.2 shows the fabricated wing molds.



Figure 4.2 Female molds for the wings

Step Three: Building the wing

First, the mold surface needs a final polishing to get a glossy surface on the wings. Second, a release agent (Frekote) is applied to the mold surface in order to allow easy separation. The third step in the wing building process is to spray a urethane based paint on the mold surface. This process provides a smooth surface on the wings. Also, the bright color of the urethane paint gives good visibility. Then, a micro Kevlar weave with low viscosity epoxy is laid over the painted surface. Next, a 0.9 mm sheet of balsa is added as a core material before another layer of the micro weave Kevlar is applied. After the Kevlar sandwich is made, a porous Teflon release filling is laid over the bottom Kevlar weave to absorb excess epoxy during the curing process. The final step in the

fabrication of the wings is to apply vacuum pressure to the layers. The layers are placed in plastic vacuum bag (as seen in Figure 4.3) and the air is pulled out, by a vacuum pump, to a suction pressure of 30 mm hg. The layers are cured for twelve hours at room temperature.

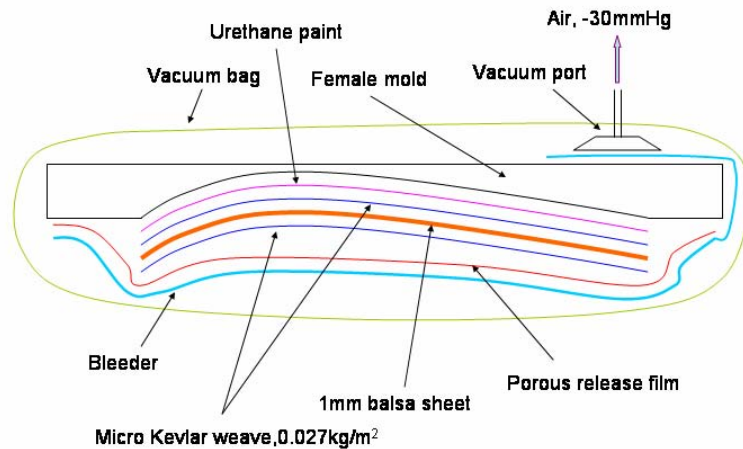


Figure 4.3 Wing manufacturing layout

After the epoxy is set, the vacuum bag and porous Teflon release are removed. The wing is ready to be assembled as shown in Figure 4.4. A balsa/carbon fiber sandwich is made for the spar and webs of the wing. Next, plywood is used to build up the area where the wing joining tube will be inserted, and for the servo mount as shown in Figure 4.4. Then, a fiberglass wing joining tube is added to give the wings moment and shearing strength. A servo with an extended wire is mounted on the plywood mount for the functionality of the ailerons. The last step in the completion of the wings is to put together the two halves. A generous amount of micro-ballooned (micro-balloons are used to save weight and thicken the mixture) epoxy is applied along the edge and on the inside of the wing structure. The wings can now be successfully joined. After the epoxy

is hard, the wing can be removed from the mold. The last step is to cut the ailerons out of the trailing edge of the wing. Figure 4.5 shows completed wings



Figure 4.4 Before wing assembly



Figure 4.5 Assembled wing and joint pipe

4.2 Fuselage Fabrication

The fuselage contains a large amount of delicate electronic components that control the airplane. A rigid fuselage is needed to protect these vital components from damage in the case of a crash. Kevlar was chosen for the fuselage because water-proof and radio communicative properties. A water-proof hatch is designed to allow access to the electrical devices.

Step one: creating of the master shape

CAD sections from ProEngineer are printed out to scale and used for the creation of bulkheads, giving shape to the fuselage. These, bulkheads are traced on sections of low-density foam as references to the actual shape of the fuse. Once all the bulkheads are sketched in, the sections of low-density foam are combined and ready to be sanded. The sanding process starts with a low-grit sand paper. A high-grit sand paper is used as the amount of foam removed gets closer to the sketch design. After the design is sanded to the correct specifications, a fiberglass weave layer is epoxied to the foam. For a smooth surface on the master shape, a layer of urethane paint is applied and polished.

Step two: making the mold for the fuselage

A Similar process is used in making the mold of the fuselage as was used in the mold of the wings (see above). Figure 4.6 shows fabricated the fuselage molds. The female fuselage molds have access holes that allow the interior to be coated with epoxy.



Figure 4.6 Female molds for the fuselage

Step three: building fuselage

First, the mold surface needs a final polishing to get a glossy surface on the fuselage. A release agent (Frekote) is then applied on the mold surface to allow easy separation. Second, clear urethane paint is sprayed on the mold so that the final product will be smooth and water-proof. Third, two layers of Kevlar weave with epoxy is laid on the wet urethane paint. Fourth, the two halves of the fuselage need to be joined. The halves are bolted together securely in order to make a one-piece final shape. The fifth step is to remove the dried Kevlar body from the joined mold. Once the mold has been removed, there are excess Kevlar overhangs that need to be trimmed down along the bodyline. The next step is to place one plywood bulkhead in the largest vertical region of

the fuselage to add rigidity. Next, a release film is placed on the center of the finished joined wings. A layer of carbon fiber is then placed on the release film and then the wing is placed in a cradle at the top of the fuselage. The carbon fiber is then measured and cut away to make a stress plate between the fuselage and wing. The four corners of the carbon fiber plate and Kevlar fuselage are tapped for the nylon wing bolts.

The final step is to insert a fiberglass tale boom in the back of the fuselage through the bulkhead and then it is epoxied into place. Figure 4.7 shows the assembled kevlar fuselage.



Figure 4.7 Fabricated fuselage

4.3 Stabilizers Fabrication

Three different iterations of the stabilizer section have been made and tested for best performance. All four stabilizers were prototyped from a CNC foam cutter. Carbon fiber was used to cover the foam stabilizers to add strength. Vertical stabilizer manufacturing follows the same procedure as the horizontal stabilizer.

The first step is to take a low-density blue foam and cut with the CNC foam cutter. The blue foam allows a narrower trailing edge to be created. Step two is to cut a piece of

Mylar release film large enough to cover the stabilizer section. Next, one layer of carbon fiber is laid on the Mylar in a scaled up version of the stabilizer. For the horizontal stabilizer, a strip of nylon weave was added along the hinge line to act as a hinge material for the operation of the elevator. Step three is to apply the carbon fiber to the foam stabilizer by folding the release material around the foam sandwiching the carbon fiber to the stabilizer. Next, the sandwiched stabilizer with Mylar covering is inserted in to the original foam cutout of the stabilizer, which is inserted into a vacuum bag to ensure proper shape deformation. Fourth step is to trim down excess carbon fiber overhang from the trailing edge of the stabilizer. Next, find the location of the nylon hinge material in the horizontal stabilizer and score along the hinge line to allow free movement. The next step is to make a tail joining assembly that correctly mounts the stabilizers in the desired angles. The fifth step is to realize the shape of the joining section on a block of yellow foam. Next, sand down the foam along a sketched design. Place a Teflon release film on the outside of the yellow foam and cover with two layers of bidirectional pre-preg carbon fiber. Cure the carbon fiber in a vacuumed environment following the heating cycles specified by the manufacture of the carbon fiber. The final step is to make a hole in both sides of the hardened tail assembly for the joining of the stabilizers. Stabilizers are mounted according to specified calculated angles. An access hole is then cut into the bottom of the assembly in order to allow the installation of the elevator and rudder servo. Figure 4.10 shows assembled stabilizer. Elevator hinge lines were created by cutting a wedge out of the underside of the stabilizer to allow deflection.



Figure 4.8 Fabricated stabilizer

All modular parts, remote controller, spare parts, and ground station fits into a 320 cm x 320cm x 1200cm wooden box. The box's total weight is about 6kg. This weight make the box able to be carried by one person.



Figure 4.9 Disassembled modular parts fit into the one man carrying box.

Figure 4.10 shows completely assembled airplane. All parts of the airplane are modularly compatible to fit together right out of the box by one assembler.



Figure 4.10 Assembled prototype WSUAV

CHAPTER 5 AVONICS

5.1 Avionics Configuration

The avionics system can be divided to three inter-related subsections. First, the Kestrel autopilot system, which is the heart of the WSUAV, consists of the autopilot, Furuno GPS and Aerocomm modem. The autopilot interfaces directly to the Aerocomm modem, which enables it to send real-time status telemetry to the ground station while receiving commands during the flight. Also it controls the three servos that control the aircraft. The second subsection, the Video system consists of 2 high resolution (greater than 500 lines) CCD cameras, a Canon Mini-DV recorder, a video overlay device, an ISM band (2.4 GHz) video transmitter and a camera switching device. When a desired camera is selected at the ground station, the autopilot applies 3V to the switching device, thereby changing the active camera. During the flight, the Kestrel autopilot provides GPS position, altitude and relative airspeed data to the video overlay device. This device displays the real-time data on the streaming video. The Mini-DV recorder provides a high-quality/low noise medium for recording and reviewing video. At the same time, the video is recorded at the ground station for real-time assessment. Due to losses in transmission and reception, the ground station recording is of lower quality. The propulsion system makes up the third subsection. It consists of an AXI brushless motor with controller, and a Lithium-polymer battery capable of providing up to 8 amperes. Through the motor controller, the autopilot maintains a given airspeed. Also, the power level of 8A polymer battery can be monitored through the ground system software.

Avionic Configuration

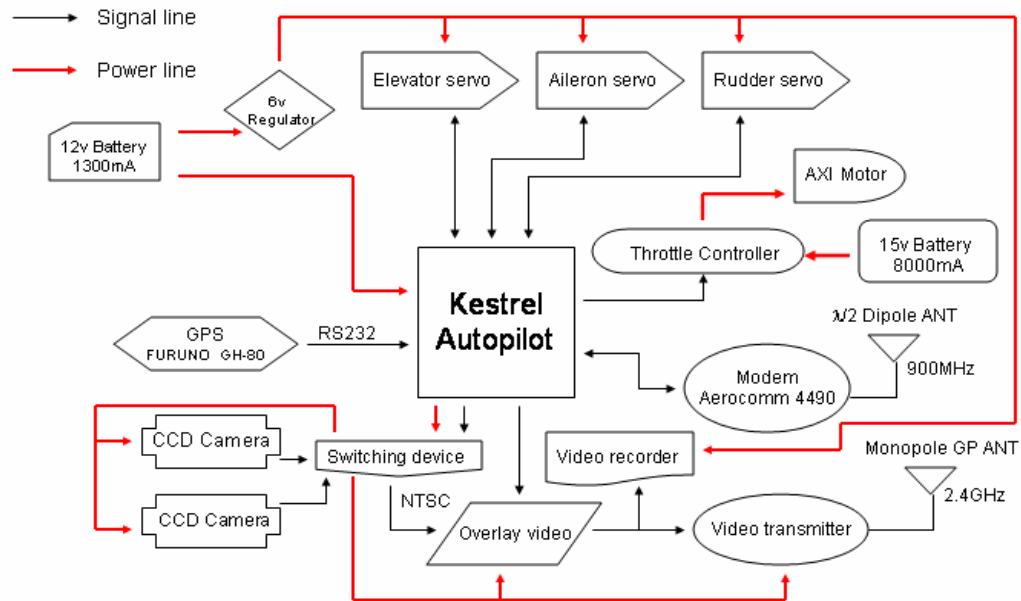


Figure 5.1 WSUAV avionics configuration

The above diagram shows how the airplane avionics are interconnected. The signal lines are narrower in width and show communication amongst that avionics. A two headed arrow depicts bi-directional communication between devices, whereas a unidirectional arrow shows single direction input or output. The power lines appear thicker and show how the 12V and 15V inputs are used throughout the system. The 12V input in combination with a 6V regulator manages the entire avionics systems except the propulsion subsystem. Due to the high current and voltage needed to drive the motor [19], a 15V 8000 mA battery is used.

Table 5.1 Electronic devices in the avionics

| | Part | Manufacturer | Ea | Type | Price/Ea (\$) | Weight (g) | Power consumption (Wh) |
|----|------------------------------|----------------|----|--------------------------|---------------|------------|------------------------|
| 1 | Parachute deploy servo | Hitec | 1 | Mini | 35 | 18 | 0.6 |
| 2 | AXI motor | Mini Motor | 1 | Casing drive | 115 | 155 | 300 |
| 3 | Controller | Jeti | 1 | Brushless | 50 | 63.4 | 1.5 |
| 4 | Elevator servo | Hitec | 1 | Mini | 20 | 25 | 0.6 |
| 5 | Aileron servo | Hitec | 2 | Flat | 60 | 30 | 1.2 |
| 6 | 1200mA autopilot battery | E2TEK | 1 | Polymer | 60 | 74 | None |
| 7 | Thunder power battery (4s4p) | Thunder power | 1 | Polymer | 300 | 645 | None |
| 8 | 1000mW Video transmitter | Black widow AV | 1 | 2.4GHz | 250 | 50 | 30 |
| 9 | Video transmitter antenna | customized | 1 | 50ohm | 5 | 7 | None |
| 10 | Canon recorder & camera | Canon | 1 | 500line progressive scan | 600 | 300 | 2 |
| 11 | CCD camera | Super circuit | 1 | 400 line | 200 | 61 | 1.2 |
| 12 | Camera switching device | customized | 1 | Relay & Regulator | 60 | 15 | 0.1 |
| 13 | Krestel autopilot | Proceduer | 1 | Rabbit processor | 4000 | 55 | 3.6 |
| 14 | GPS | Furuno | 1 | Micro | 80 | 18 | 0.5 |
| 15 | Regulator | Powerflite | 1 | 6v | 30 | 15 | 0.1 |
| 16 | Video overlay device | UNAV | 1 | 12v | 120 | 33 | 0.8 |
| 17 | Modem | Aerocom | 1 | 900Mhz | 90 | 20 | 1.5 |
| 18 | Modem antenna | customized | 1 | Dipole | 10 | 9 | None |
| 19 | Autopilot wire bundle | Proceduer | 2 | Micro | 10 | 8 | None |
| | Total | | | | 6095 | 1601.4 | 343.7 |

Table 5.1 above shows the complete inventory of the avionics system. The table also provides specifications for each component. Total power consumption is used to calculate flight duration. The total avionics system costs about \$6,100 which is satisfactory for an inexpensive WSUAV.

5.2 Kestrel Autopilot System

The Kestrel autopilot system can be divided into airborne components and ground station components (Figure 5.2). The airborne components consist of the autopilot, GPS, and data link modem. The ground station components are ground station software and hardware.

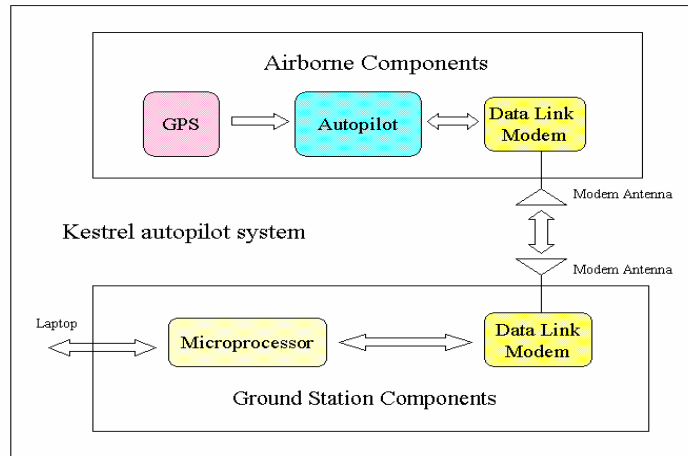


Figure 5.2 Kestrel autopilot system

Autopilot

The autopilot shown in figure 5.3 is operated by an 8-bit 29 MHz Rabbit microprocessor and contains a suite of sensors, 3axis piezo gyros, accelerometers, and pressure sensors, used by the autopilot software to measure and estimate of the airplane attitude and location through the sensors.

Figure 5.4 shows the Kestrel autopilot ground station that communicates with the onboard autopilot in the plane via a data link modem that operates on 900 MHz spread spectrum. This device also uses a Rabbit microprocessor like the one onboard the plane's autopilot to control data.



Figure 5.3 Kestrel autopilot



Figure 5.4 Kestrel autopilot ground station

GPS

The Furuno GPS presents velocity, heading, and position information necessary for waypoint navigation with binary format.

Data Communication Link

The modem allows real time communication with the ground station. A $\lambda/2$ dipole antenna is used on the aircraft. The autopilot helps communication with a digital modem running at 115 Kbaud. The Aerocomm AC4490 modem has a 115 Kbaud interface and supports a 57600 Kbaud over-the-air rate and a 1000 mW power output. Communication ranges of larger than 10 kilometers can be attained. The modems have tested out to a range of 5 kilometers with minimum packet loss.

5.2.1 Autopilot Control Theory

Lateral Control

WSUAV doesn't have a rudder in order to simplify its control; therefore yaw rate control is not required in autopilot.

The lateral controller is responsible for controlling the yaw rate, roll angle, and heading. This is accomplished with two inner servo loops and one outer loop. The inner loops drive the aileron, and the outer loops produce commanded values for the inner loops. The inner lateral loops are as follows:

1. Aileron rate control from roll rate: this loop produces an aileron deflection from the roll rate and is summed with the effort from the Aileron from roll loop and sent to the aileron servo as shown in Figure 5.5. It is in charge of dampening the roll rate of the aircraft.
2. Aileron rate control from roll: This loop produces an Aileron deflection from the roll error, and manages to hold the roll attitude of the aircraft, as shown in Figure 5.5.

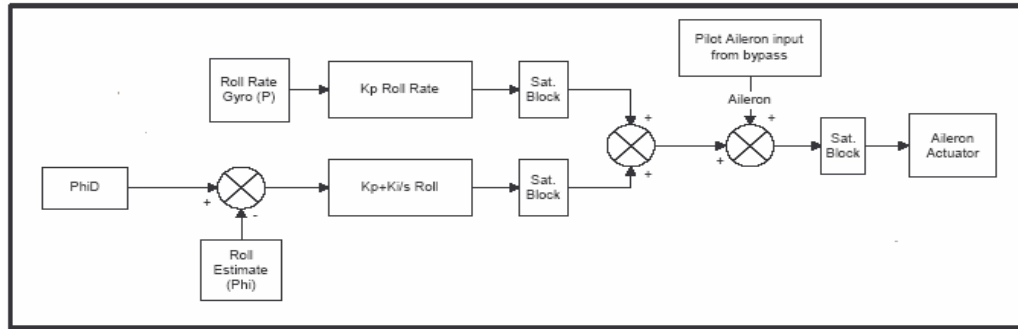


Figure 5.5 Roll rate controller and inner lateral roll

The outer lateral control loop is the following:

1. Roll from heading: This is the loop used to control the heading of the aircraft. It generates a roll angle from the heading error as shown in Figure 5.6. This roll angle serves as the commanded roll angle for the aileron from roll loop.

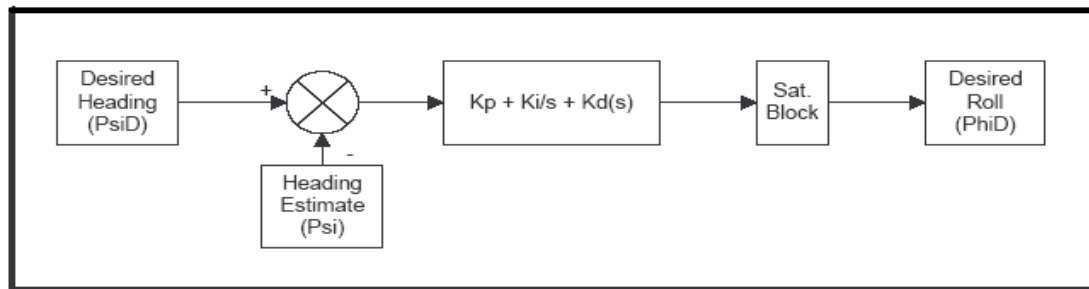


Figure 5.6 Outer lateral heading angle controller

Longitudinal Control

The longitudinal controller is in charge of controlling the pitch angle, velocity, and altitude. This is accomplished with 2 outer loops and 3 inner servo loops. The inner loops drive the elevator and throttle, and the outer loops produce commanded values for the inner loops. The inner lateral loops are as follows:

1. Elevator from pitch rate: This loop generates an elevator deflection from the pitch rate. It is responsible for dampening the pitch rate of the aircraft.

This loop's control effort is summed with the elevator from the pitch loop and sent to the elevator servo actuator. See Figure 5.7.7

2. Elevator from pitch: This loop produces an elevator deflection from the pitch error as shown in Figure 5.7 and is in charge of holding the pitch attitude of the aircraft.

3. Throttle from airspeed: The purpose of this loop is to control the aircraft's speed by controlling the throttle. This loop drives the throttle servo as shown Figure 5.8.

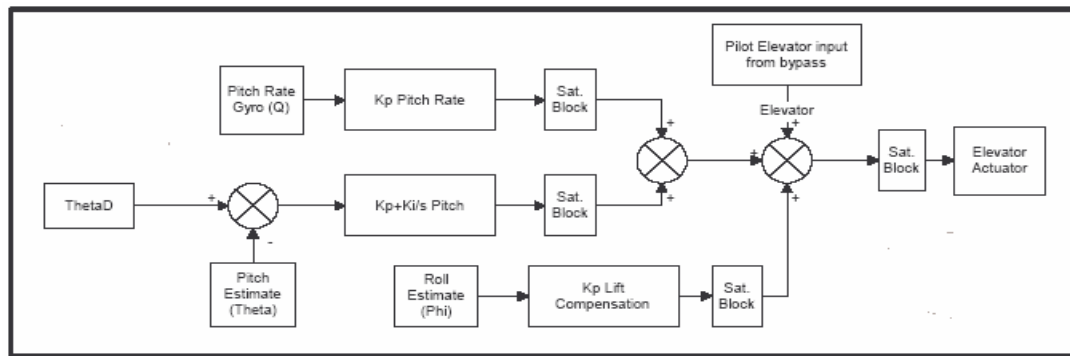


Figure 5.7 Inner longitudinal pitch and pitch controller

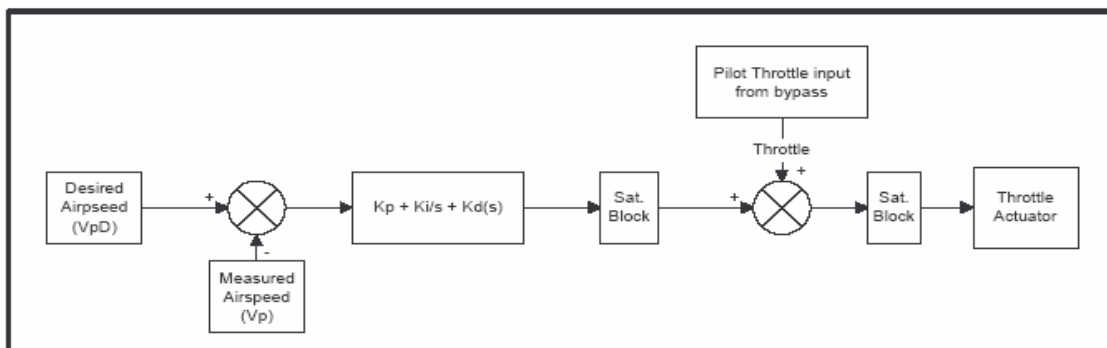


Figure 5.8 Inner longitudinal airspeed controller

The outer lateral control loops are as follows:

1. Pitch from altitude: This loop produces a controlled pitch angle from the altitude error.

From this, the loop joins directly to the elevator from pitch loop.

2. Pitch from airspeed: This loop controls the aircraft's speed by adjusting the pitch angle. The output of this loop connects directly to the elevator from pitch loop. This loop is used to regulate the aircraft's airspeed during climb and descent. This loop is shown in Figure 5.10.

3. This loop is suitable for controlling the aircraft's altitude when the altitude error is small, as shown in Figure 5.9. The pitch from airspeed loop should be used at large altitude inaccuracies.

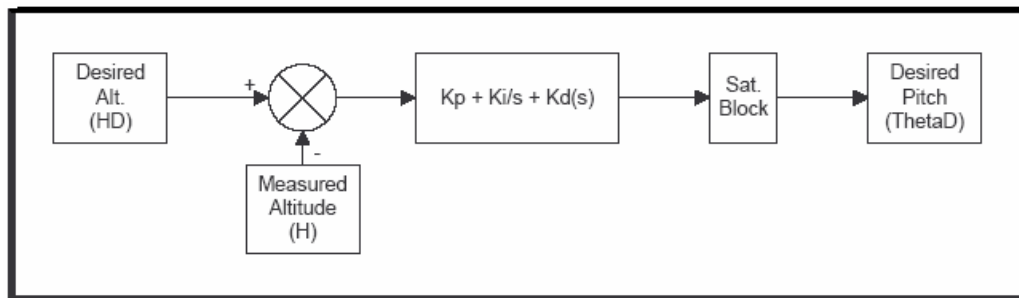


Figure 5.9 Outer longitudinal altitude controller

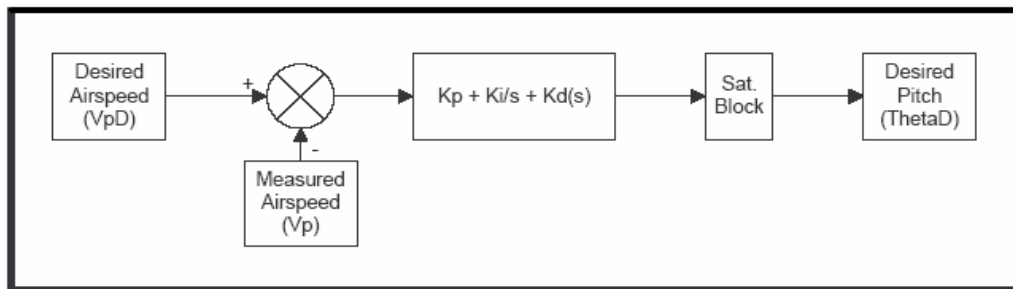


Figure 5.10 Outer longitudinal airspeed controller

5.2.2 The Virtual Cockpit Software

A graphical interface was written to control the autopilot. The graphical interface software is called as the virtual cockpit. The virtual cockpit is a complete system that is used to configure, debug, program, and monitor the autopilot as shown in Figure 5.11.

The virtual cockpit encloses several screens accessible by tabs and a Status screen that is always visible. The purpose of the Status window is to give the user an indication of the aircraft's status and health. The virtual cockpit has 4 tab windows, which contain specific control and setup information.

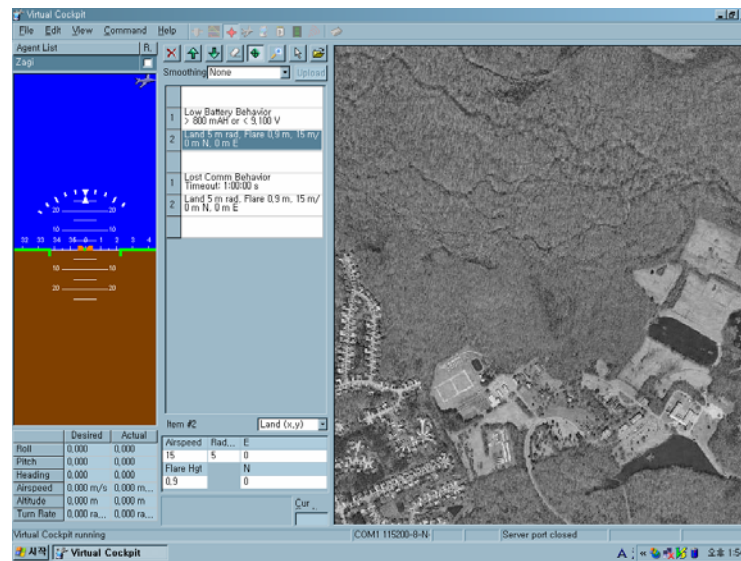


Figure 5.11 The virtual cockpit software

5.3 Camera and Recording System

Most UAVs have two cameras or one camera with a gimbaled system (pivotal in 2 axes) for transmitting video images to the ground station. In a two-camera configuration, one camera captures a front-down (camera angled about 10 degrees) view and the other camera displays a bird's eye view. A front-down view is preferable for a military reconnaissance mission because it allows the pilot to see what the plane is seeing and therefore allow better navigation. For wildlife surveillance, the bird's eye view can be used for population estimations in a finite area. Some WSUAV's can have a side-mounted camera that can be used to loiter over a particular GPS location at a set bank angle in order to examine animal behavior closely. A gimbaled one-camera

configuration can obtain relative target position from the gimbaled camera angle, GPS coordinates, and altitude readings. However, this gimbaled angle reading is unreliable in poor weather conditions and is susceptible to water damage in water landing applications. Hence, a bird's eye view and side view camera configuration is preferable for the WSUAV. The bird's eye view camera should be mounted in a safe location and should not obstruct landing procedures in order to prevent damage to the camera. Table 5.2 shows two selected cameras because of its higher price verse performance. To obtain a more reliable image, video can be recorded into an on-board recording device. Figure 5.14 shows this device as a trim-downed size and weight.

Table 5.2 Cameras specification as shown in Figure 5.12 and 5.13.

| Name | Location | Resolution | Shutter speed | Power |
|-----------|----------|------------|----------------|-------|
| KPC-S900C | Side | 380line | 1/60–1/100,000 | 12V |
| EUREKA | Bottom | 500line | 1/50–1/100,000 | 6V |



Figure 5.12 500 lines resolution CCD camera for the bottom view.

The camera is located in the rear on the bottom of the fuselage. This location keeps the camera protected during landings.

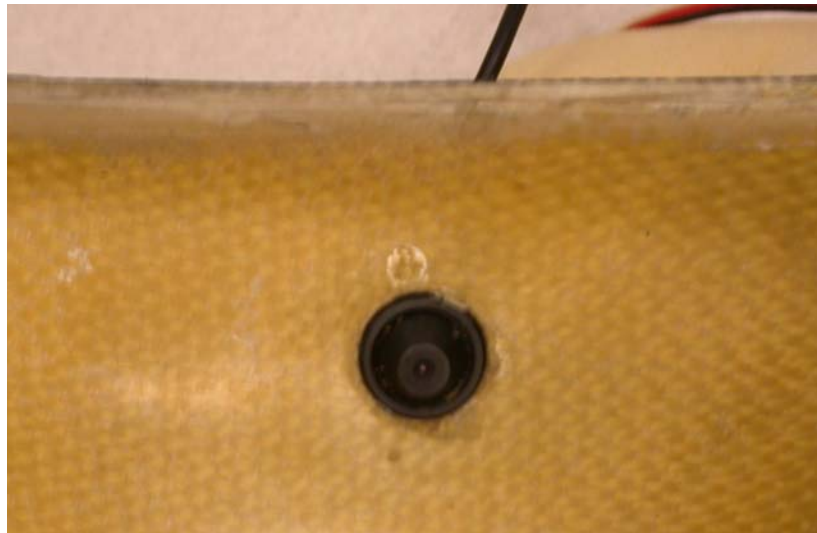


Figure 5.13 380 lines resolution CCD camera for the side view

The camera is located on the left side of the plane just under the wing. The camera is installed at a slight 20 degree down angle.

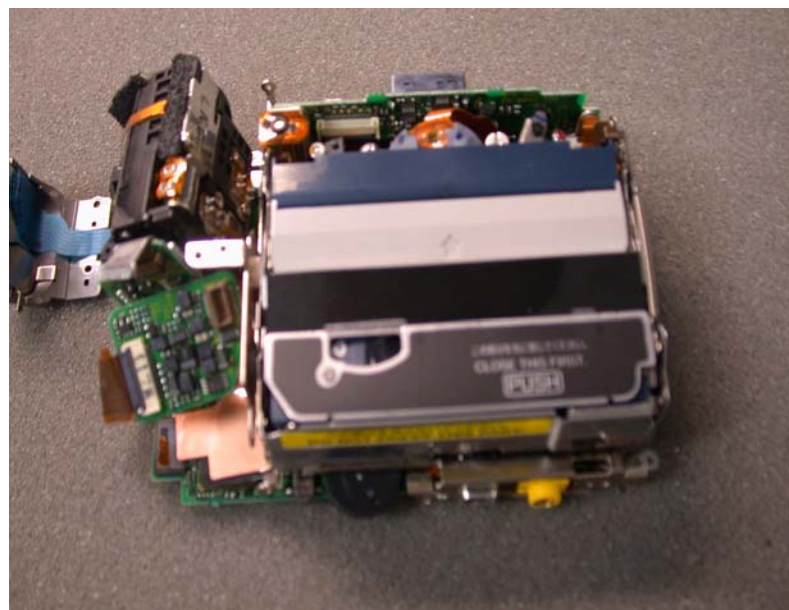


Figure 5.14 Video recording device.

This video recording device has been modified from its original camcorder setup in order to save size and weight. This recorder records on a mini-DV sized media. This device is controlled from the ground station and has recording times up to 2 hours in length.

5.4 Ground Plane (GP) Antenna Design for Video Transmitter

Antennas in WSUAV

The WSUAV uses three different kinds of antennas. A video-transmitting antenna operates at 2.4 GHz and transmits real-time video to the ground station. The Data link antenna operates at a spread spectrum of 900 MHz and transmits real-time navigation data as well as other various airplane operations to a ground station. The GPS unit in the plane is passive and receives information via GPS satellite. A damaged antenna can cause a reduction in signal transmission or reception in distance. In particular, a damaged Data link antenna contributes to a data package loss to the ground system.

Ground Plane (GP) Antenna Design

Most commercial video transmitters come with wavelengths (W) of the order $\lambda/2$ dipole and monopole antennas that are designed to have symmetric radiation patterns for getting rid of dead spots during the airplane's flight (Figure 2). Despite the transmitter's high output (more than 1 watt) and symmetric radiation pattern, the ground station frequently loses video signal, which has been proven by many flight tests. This can attribute to the fact that most of these commercial antennas are designed for applications on the ground, and not for use in aerial environments. Even though a high output transmitter has more than enough range to cover a couple of miles, it is not able to do so because of these antennae issues. Hence, we can increase video range by changing the frequency radiation downward from the antenna. This is the reason for using a $\lambda/2$ dipole

antenna. The intended frequency pattern of the $\lambda/2$ dipole antenna is that of two circles that barely overlap. The pattern that is observed in flight however, is a somewhat coarse circular pattern. Whenever the airplane goes outside of this enclosed area, it experiences what is known as a dead region. This forces flight within a much tighter circle and reduces loss of communication with the transmitter. The center of this combined figure represents the position of the airplane in flight (Figure 5.15 upper side). When the ground station is located far below the airplane during flight, all transmitted frequency that exists above the antenna is wasted. This excess transmission consumes more power for less range. From the top to the center of both concentric circles also represents the upper limits through which the dipole antenna will transmit energy. The GP antenna provides a bigger circle and downward pattern that provides a wider and more accessible region within which the airplane can fly without experiencing any dead zones. The middle three ground planes have a 120° symmetric radiation pattern. Also between each ground plane and monopole antenna there is a 120° downward radiation pattern, as shown in the top of Figure 5.15.

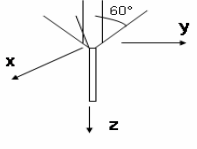
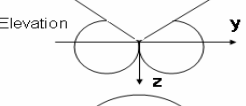
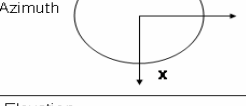
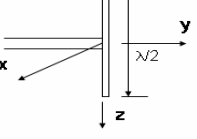
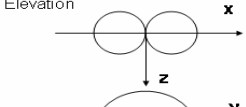
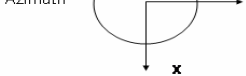
| Type | Radiation Pattern | Characteristics |
|------------------------------------------------------------------------------------------------------------|----------------------------------------------------------------------------------------------------------------------------------------------------------------------------------------------------|-------------------------------------------------------------------------------|
| Monopole GP Antenna  | Elevation  Azimuth  | Typical Gain: 2-6dB Polarization: vertical ,linear |
| $\lambda/2$ Dipole  | Elevation  Azimuth  | Typical Gain: 2-3dB Polarization: vertical ,linear |

Figure 5.15 Comparison of antenna radiation pattern

Figure 5.16 below shows a modified monopole antenna with 120 degree ground planes fabricated from copper strips. This 3-prong ground plane assembly emits a symmetric radiation pattern.

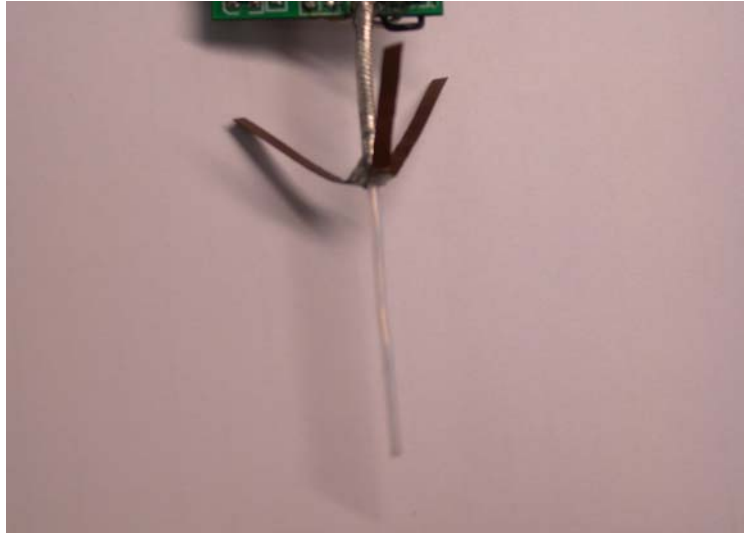


Figure 5.16 Fabricated and calibrated GP antenna

Calculations for GP antenna design

Video transmitter frequency: 2.453 GHz

$$= 2.453 \times 10^9 \text{ [cycles/sec]}$$

$$W = C \times T$$

$$W \text{ [meters]} = 3.0 \cdot 10^8 \text{ [meters/sec]} \cdot T \text{ [sec]}$$

$$T \text{ [sec/cycle]} \cdot 2.453 \cdot 10^9 \text{ [cycles/sec]} = 1$$

$$T = 1 / (2.453 \cdot 10^9)$$

Using the equation in terms of W for 2.453 GHz:

$$W \text{ [meters]} = 3.0 \cdot 10^8 \text{ [meters/sec]} \cdot (1 / 2.453 \cdot 10^9 \text{ [cycles/sec]})$$

$$W = 3.0 \cdot 10^8 \cdot 2.453 \cdot 10^{-9} \text{ [meters/cycle]}$$

$$= 3.0 / 2.453 \cdot 10^{-1} = 12.5 \text{ cm}$$

Hence, GP monopole antenna length:

$$W = \lambda, \lambda/4 = 3.125\text{cm}$$

Where, C: the speed of light $= 3.0 \cdot 10^8$ m/sec

T: Time

W: Wavelength

F: Frequency (cycles per second)

Actual calibrated GP monopole antenna length: 3.2cm

Calibration and evaluation of the fabricated GP antenna

A resonant line may be determined from a short circuit, a capacitor, an open circuit, a resistor, or an inductor that may not be part of the characteristic impedance of the antenna. In any such case, some of the transmitted energy is reflected back to the source and forms standing waves on the line because the line cannot deliver maximum energy to a load. On a resonant line, some of the energy sent down the line will be reflected back to the transmitter, resulting in standing waves. Along the resonant line, high voltage and low current points appear. Hence, commercial antennas, with wavelengths (W) of the order $\lambda/2$ dipole antennas are widely used in 2.4 GHz ISM band video transmitters.

The GP antenna can be calibrated by using a network analyzer shown in Figure 5.17 to match the impedance by the length of the antenna and ground plane's length and size. We can recognize antenna impedance by the Smith chart on the network analyzer. Network analyzers can show that one antenna can and does serve for more than one frequency, but generally the ones in the middle of this frequency range will work better than the ones on the ends. Hence an antenna should be designed around the middle of the

band you are working with so that it will work more efficiently. Impedance is required to be 50 ohms because the main RF barrel is actually a special coaxial line segment with 50-Ohm characteristic impedance. Normally, impedance is determined by the particular combination of resistance, inductive reactance, and capacitive reactance in a given circuit.



Figure 5.17 Network analyzer showing impedance matching for the GP antenna

Figure 5.17 shows a 48ohm measured impedance from the Network Analyzer can determine the reflection coefficient (RC). This is the ratio of the amplitude of the reflected wave to the amplitude of the incident wave. The perfect condition of no reflection occurs only when the load is purely resistive and equal to Z_0 . Such a condition is called a flat line and indicates a Standing Wave Ratio (SWR) of 1.

$$RC = \frac{Z_1 - Z_2}{Z_1 + Z_2} = \frac{SWR - 1}{SWR + 1} = 0.024$$

Where, Z_1 is the impedance toward the source and Z_2 is the impedance toward the load.

Z1: measured GP antenna impedance, 48ohm

Z2: 50ohm

$$\text{Return loss} = -20 \log RC = 34.29$$

Return loss is obtained from the RC value. If the return loss is greater than 30, the antenna is performing well.

5.5 Video Reception Maximization at the Ground Station

To determine the maximum gain combination with a Low Noise Amplifier (LNA) and the receiver antenna, a spectrum analyzer is used to test a number of antennas and LNAs. The results were measured from a distance of 100ft using the RF link transmitter SDX-22LP (2.453 GHz, 80mW). Table 5.3 shows a list of antennas and their output power. The LNA increases the gain of a receiver without adding a large parabolic antenna; this can simplify the ground system. The customized LNA has a high gain operating at 12V 60 mA. In Table 5.3, the patch antenna model A2.45FP12 with customized LNA pictured in Figure 5.19 was found to be the best-chosen antenna. Its reception power level was tested on a spectrum analyzer and was compared to the worst antenna and LNA combination. The results are displayed in Figure 5.18.

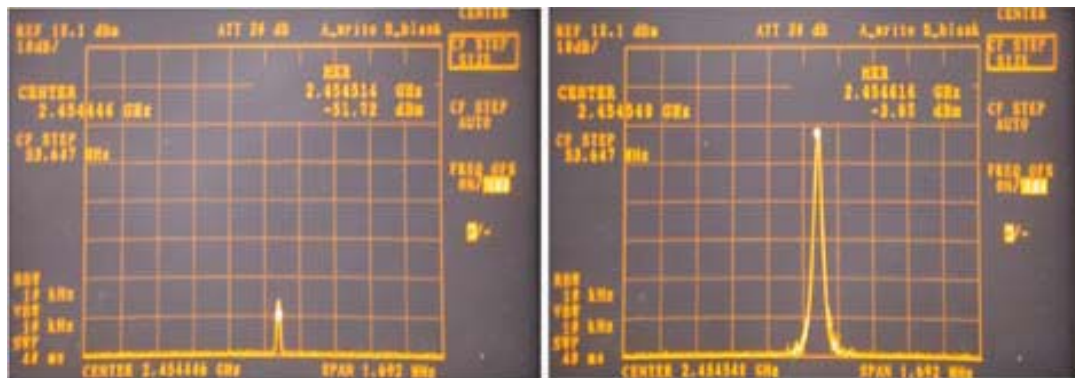


Figure 5.18 The Spectrum analyzer output before (left) and after (right) use of customized LNA

Table 5.3 Antennas comparison of output power

| Antenna Model | Without LNA (dBm) | With LNA (ZFL-VH) (dBm) | With customized LNA (dBm) |
|--------------------------------|-------------------|--------------------------|---------------------------|
| A2.45FP12 (patch antenna) | -51.72 | -31.23 | -3.93 |
| HG2414P (patch antenna) | -53.28 | -47.2 | -21.17 |
| MVR-4 (patch antenna) | -58.24 | -41.03 | -7.03 |
| ODP-2400 (omni-directional) | -55.72 | -43.3 | -13.2 |

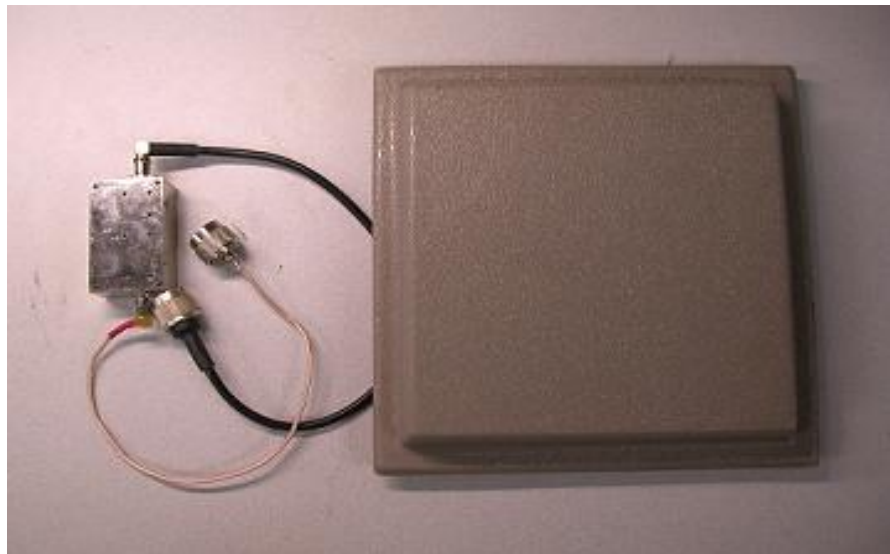


Figure 5.19 Model A2.45FP12 antenna with a customized LNA

Figure 5.20 shows an overview of how Radio Frequency (RF) communication between the airplane's transmitting antenna (sends a real-time video feed) and the ground station's receiving antenna functions through free space. The figure shows losses in free space and in both transmission lines.

Schematic Diagram of a RF System

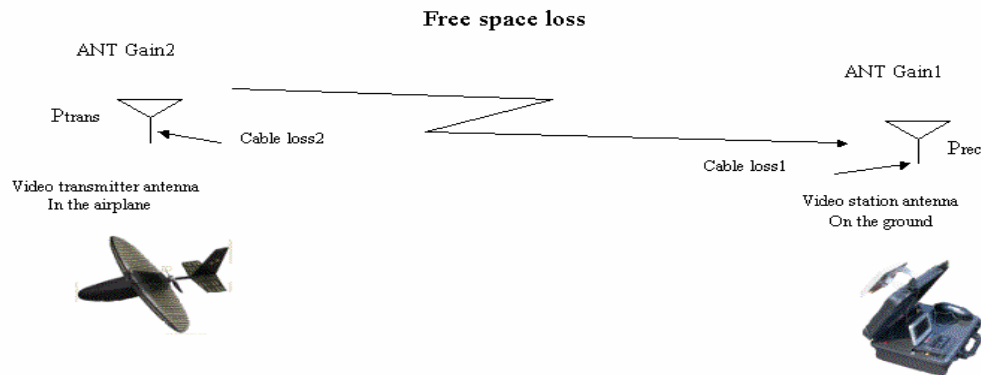


Figure 5.20 Schematic diagram of a video transmission

The following equations are used to calculate final reception power (dBm) in the video transmitting antenna.

The equation for output power, dBm is given by:

$$dBm = 10 \log \frac{P_o}{P_i}$$

Po: Power out of the system

Pi: Power into the system

$$P_{rec} = P_{trans} - \text{Gain 1} + \text{Gain2} - [\text{Loss 1} + 10 \log (Q1) + \text{Fsl} - 10 \log (Q2) + \text{Loss2}]$$

Where, P_{rec} : received power

P_{trans} : total transmitted power

Loss1 and Loss2: transmission line losses

Gain 1 and Gain2: receiver and transmitter antenna gains, respectively

Q1 and Q2: used to calculate the additional losses due to mismatch

Fsl: free space loss

5.6 Camera Switching Device Design and Fabrication

In today's market, most CCD cameras and video transmitters require different power sources to function properly. Some common examples are models which use 5V, 6V, and 12V sources. For the purpose of the WSUAV, a Kestrel Autopilot system generates a 3V, 20 mA power source whenever an active command for changing from one camera to the other is given from the ground-station or pre-programmed. A 12V micro camera switching device (powered from the Kestrel Autopilot) was conceived which controls two independently operating cameras based on autopilot output. By using these micro components, the overall design of the camera switching device is reduced in terms of size, weight, and complexity. The output channel of the autopilot produces an insufficient amount of power to activate the Teledyne ER412D switching relay, so the power needs to be stepped up from 3V, 20mA to 5V, 200mA by means of a 2N7000 transistor. This new power output will energize the relay alternating the signal from a default camera (at a non-energized state) to the other camera. The chosen camera signal is routed through the relay to a single video transmitter. The camera switching circuit also has an option to select different input voltages by means of a jumper pin. This feature is especially important for WSUAV because the use of different kinds of cameras might be necessary depending on the application. Certain cameras require different input voltages: either 5V or 12V.

The circuit was consolidated onto a printed circuit board. The layout of the circuit board was designed by Protel DXP2004 software as shown Figure 5.21. A rendering of the drill-hole pattern, line trace pattern, and silk screen pattern as shown in Figure 5.23 were then electronically forwarded to Advanced Circuits for board

fabrication. Note that the camera (CA) and video transmitter (V.T.) connectors at the lower portion of the figure are jumpers that allow the use of either 12V or 5V video equipment. 5V equipment is powered from the Burr Brown 5V regulator shown in the figure (BB1175). Figure 5.22 shows the fabricated circuit board populated with the discrete components. The circuit board is sized to 28 mm x 30 mm and a weight of 12g.

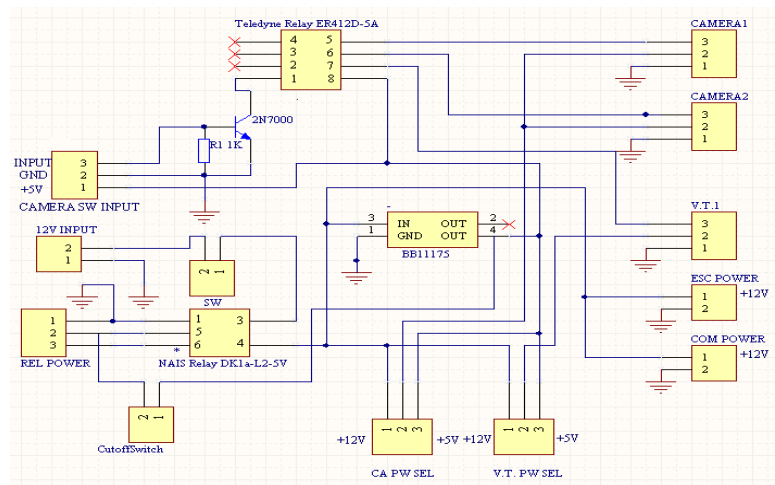


Figure 5.21 Camera switching device schematic

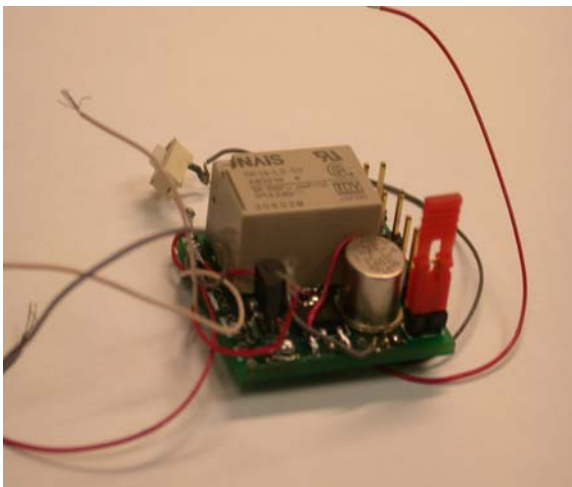


Figure 5.22 Assembled camera switching device.

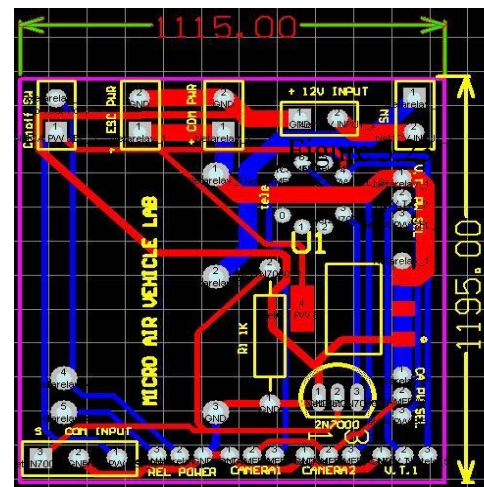


Figure 5.23 Printed circuit board layout.

CHAPTER 6 AIRPLANE EVALUATION

6.1 Propulsion Evaluation

For the propulsion system and flight performance evaluations, the RCATS telemetry device was used. The RCATS device was used because the onboard autopilot system is incapable of collecting RPM measurements, as well as measurements on the power consumption of the propulsion system. RCATS is developed around a 20MHz micro controller-based system that collects data from numerous sensors. The data, which is displayed and recorded in real time, is then relayed through a Radio Frequency modem to a receiver on a ground based laptop display at 4Hz. All sensors, pressure, rpm, voltage, and current sensors, must be calibrated before the test flight.

The AXI 2820/20 brushless motor, Thunder power 8020 battery and Jeti speed controller were used for the drive and power source section of this test, while the APC 10-7E (250mm long, 175mm pitch) and APC 9-6E (225mm long, 150mm pitch) propellers (designed for electric motors) were used to compare climb rate and total efficiency. Before flying, for accuracy, the pressure sensor was calibrated to zero at ground level. The manufacturer's specifications of resolution error are approximately +/- 2m altitude, +/- 1V voltage, and +/- 1 Ampere current resolution. The slope lines, shown in Figures 6.1 and 6.2, both show a reasonably linear climb rate. These tests were done in about +/- 1m/s headwind conditions, while the total gross weight of the airplane (3.2 kg) was kept constant.

6.1.1 Comparison of Climb Rate at takeoff

The comparison of the two climb rates were taken up to 70 meters in altitude from the ground. This altitude is the minimum mission capable altitude from the ground. The power curve, in Figures 6.1 and 6.2, show the power consumption in the propulsion system. It oscillates because of unreliable sensing resolution during the flight test. Therefore, average values are used for calculation's involving total power. During the tests, the elevator deflection the drive and power sources (100% battery power) were kept constant.

Test with APC 9-6E propeller

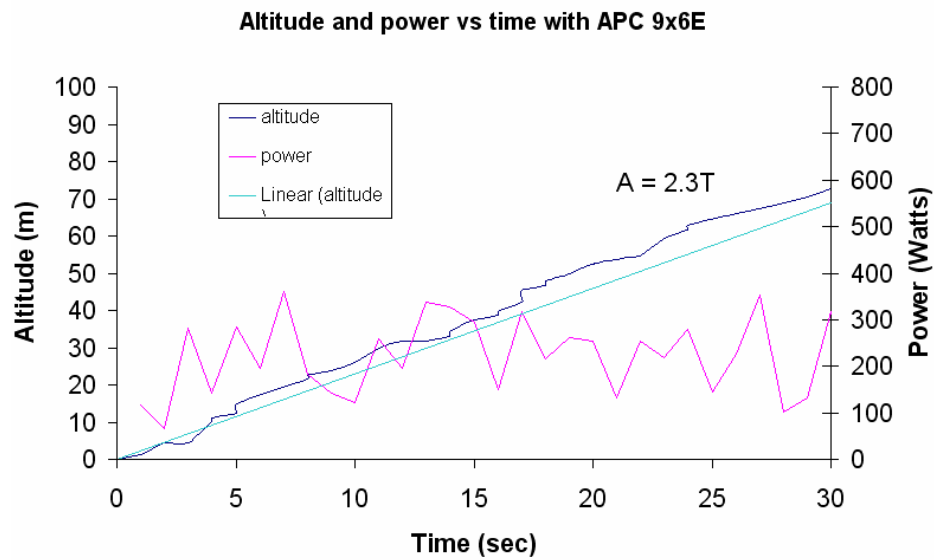


Figure 6.1 Takeoff profile with APC9-6E propeller, graph shows climb rate and power consumption by propulsion system during takeoff up to 70m altitude.

Figure 6.1 above shows the take-off profile of the WSUAV with the APC9x6E propeller at ground altitude of 50 m above sea level. The data captured during takeoff is model by a slope of linear trend line, $A=2.3T$. We have an average climb rate (m/s) by the derivative of this slope.

$$\text{Average climb rate (m/s)} = \frac{\partial A}{\partial t} = 2.3 \text{ m/s} \quad \text{Where, } A = 2.3T$$

The total power consumption is the power consumed during takeoff up to a 70 m altitude.

Average power consumption and total time are obtained from Figure 6.1 during a 28 sec climb, using 199.6 W. Total power consumption, Wh, is expressed as following:

$$Wh = W \cdot h \quad (6.1)$$

Where Wh is total power consumption, W is average power consumption, and h is flight time in hour. Using equation 6.1, we can obtain total power consumption. During takeoff the power consumed was 1.55 Watt hours.

Test with APC 10·7E propeller

The test of the APC 10·7E propeller was taken using identical conditions as the 9·6E propeller. Figure 6.2 shows a 2.25 m/s average climb rate during 29 sec up to 70 m altitude and 544.7 W average power consumption into during 29 sec.

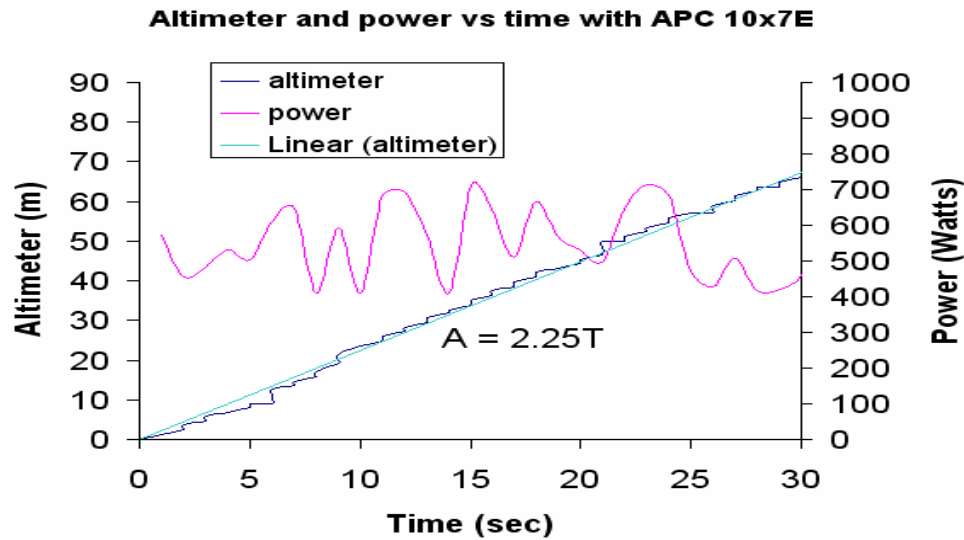


Figure 6.2 Takeoff profile with APC10·7E, graph shows 2.25 m/s climb rate

Figure 6.2 the data captured during takeoff is model by a slope of linear trend line, $A=2.25T$. We have an average climb rate (m/s) by the derivative of this slope.

$$\text{Average climb rate (m/s)} = 2.25 \text{ m/s} \quad \text{Where, } A = 2.25T$$

$$\text{Total power consumption} = 4.39 \text{ Wh}$$

Both conditions, with APC 9-6E and 10-7E are satisfactory for the given requirements (2 m/s) and have a reasonably linear climb rate, but 10x7E configuration shows higher total power consumption.

6.1.2 Comparison of efficiency at cruise

Test of the APC 9-6E propeller

The total efficiency in the propulsion system with the APC 9x6E propeller is calculated using the average speed and the average altitude shown in Figure 6.3. Total efficiency of the propulsion system is the product of the four elements: Propeller, motor, speed controller, and battery. The battery efficiency for comparing the two different propeller configurations will be assumed to be 1. Power input from the battery for both testing configurations was negligibly different. From Figure 6.3, we can obtain the following parameters:

RPM: revolution per minutes of propeller = 11,112 /sec

η_{motor} : efficiency of motor = 0.75 at 20-30A range from Table 3.6

η_{esc} : efficiency of electronic speed controller = 0.95 from the specification.

η_{total} : total efficiency of propulsion system = $\eta_{\text{motor}} \cdot \eta_{\text{esc}} \cdot \eta_{\text{prop}}$

P_{Min} : input power into the motor through the electronic speed controller = 294.4 W

P_{Mout} : output power from the motor = $P_{\text{Min}} \cdot \eta_{\text{motor}} \cdot \eta_{\text{esc}} = 209.8 \text{ W}$

V_{ave} : average velocity of airplane during cruise = 16.2 m/s

A_{ave} : average altitude during cruise + ground level altitude (50m) = 124.5 m

$\rho_{alt} = 1.2 \text{ kg/m}^3$, air density at 124.5 m

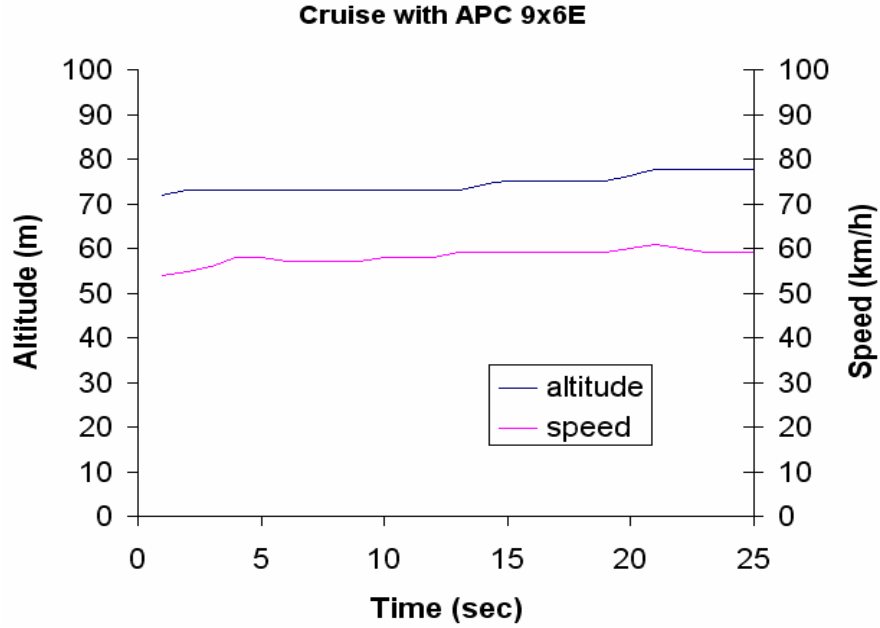


Figure 6.3 Graph shows altitude and flight speed variation during 25sec cruise

with APC 9-6E propeller.

The calculations below take the average velocity, propeller diameter, output motor power, and air density from the altitude data to give us propeller efficiency, η_{prop} .

At different average velocities the propeller efficiency will change according to Figure 6.5.

$$V_{ave} = \eta_{prop} \cdot \left(\frac{2 \cdot P_{Mout}}{\pi \cdot \rho_{alt} \cdot D^2 \cdot (1 - \eta_{prop})} \right)^{\frac{1}{3}} \quad (6.2)$$

Efficiency of propulsion system, η_{total} , is obtained from Equation 6.2

$$\eta_{total} = \eta_{motor} \cdot \eta_{esc} \cdot \eta_{prop} \quad (6.3)$$

Thrust, T can be obtained with efficiency of propulsion system previously.

$$T = \frac{P_{Mout} \cdot \eta_{total}}{V_{ave}} \quad (6.4)$$

Using Equations 6.2-6.4, the efficiency of the APC 9-6E propeller amounted to 77% while the efficiency of the propulsion system was 55%. The calculated thrust of the propulsion system was 7.12 N.

Test of the APC 10-6E propeller

During the test, about 10 m altitude climb is observed with in Figure 6.4 below. It decrease overall efficiency values in propulsion system but this propeller and propulsion configuration still show higher efficiency than APC 9-6E propeller configuration with results as shown in Figure 6.5 and 6.6.

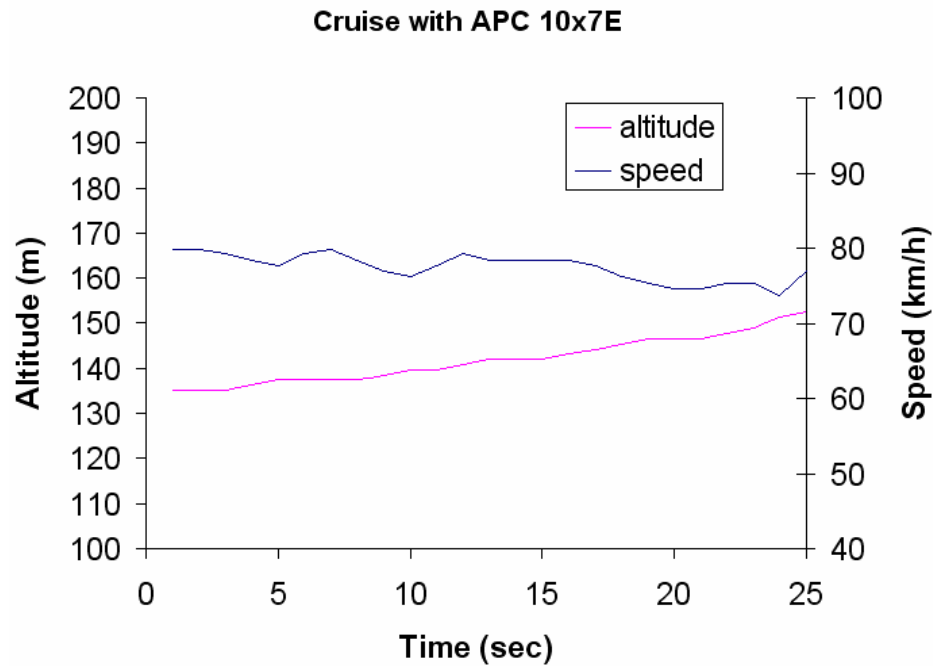


Figure 6.4 Graph shows airplane's altitude and flight speed variation during 25sec cruise with APC 10-7E propeller.

From Figure 6.4, we can obtain the following parameters:

$$\text{RPM} = 10829 \text{ /sec}$$

$$\eta_{\text{motor}} = 0.75$$

$$\eta_{\text{esc}} = 0.95$$

$$P_{\text{Min}} = 346.3 \text{ W}$$

$$P_{\text{Mout}} = P_{\text{Min}} \cdot \eta_{\text{motor}} \cdot \eta_{\text{esc}} = 246.7 \text{ W}$$

$$V_{\text{ave}} = 21.46 \text{ m/s}$$

$$A_{\text{ave}} = 192.5 \text{ m}$$

$$\rho_{\text{alt}} = 1.202 \text{ kg/m}^3, \text{ air density at } 192.5 \text{ m}$$

Efficiency of the APC 10-7E propeller amounts to 85%, while the efficiency of propulsion system is 60%. The thrust of the propulsion system is 6.89 N using the correlations in Equation 6.2, 6.3, and 6.4.

Both Figures 6.5 and 6.6 were plotted with Equation 6.2. By observation of following graphs, two different propellers have a closely related propeller efficiency in the desired air speed (22 m/s) but APC 10-7E illustrates higher efficiency at air speeds above the desired air speed.

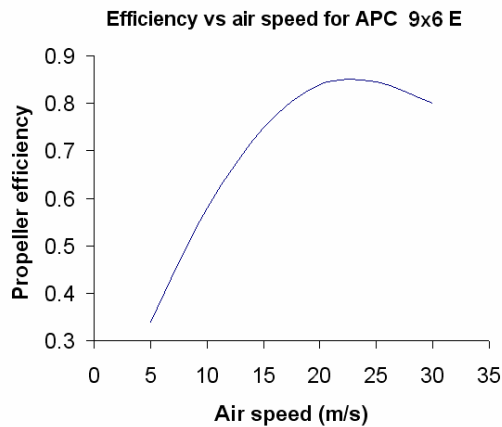


Figure 6.5 Propeller efficiency of APC 9-6E

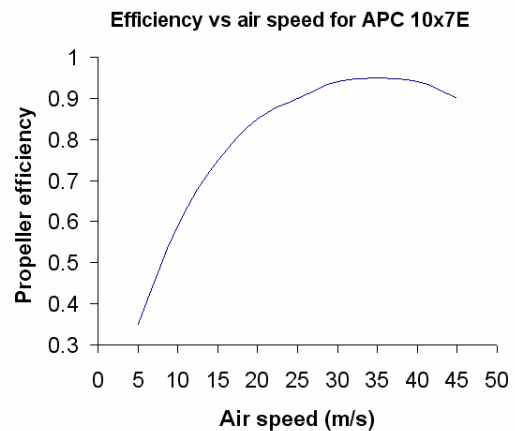


Figure 6.6 Propeller efficiency of APC 10-7E

6.2 Autopilot Evaluation

Lateral Autopilot Simulation

For a test bed, simulation of the closed loop lateral performance of the onboard WSUAV autopilot was used. To do this, an inner roll PID loop was simulated by giving a step input in the desired roll angle (Φ). This can be seen with the dotted line as the desired roll angle and the solid line as the actual response in Figure 6.7. By observation of Figure 6.7, it is obvious that the performance of the autopilot can be effectively obtained with PID control during its time in lateral modes.

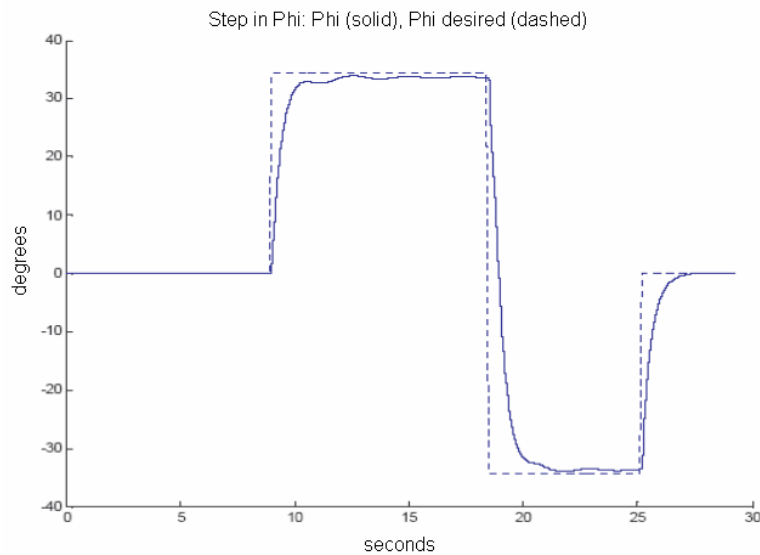


Figure 6.7 Closed loop lateral response to step in desired roll angle (Φ).

Longitudinal Autopilot Simulation

The closed loop longitudinal performance of the onboard WSUAV autopilot was simulated in the inner pitch PID loop, which is transcribed by giving a step input in the desired pitch angle (Θ). The results can be seen in Figure 6.8. This testing data shows

that in response to step inputs, the PID mode can effectively control the WSUAV's pitch angle.

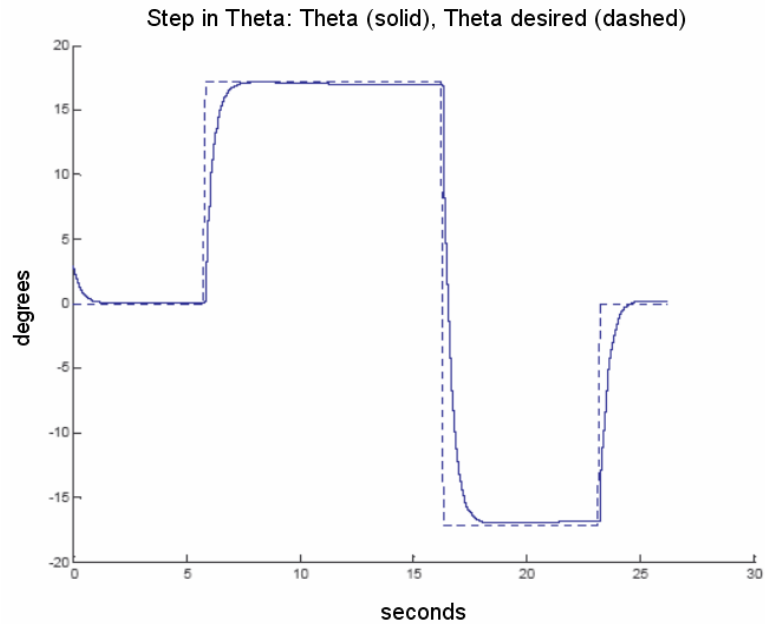


Figure 6.8 Closed loop longitudinal response to step in desired pitch angle (Theta).

GPS Waypoints Navigation Simulation

Figure 6.9 shows the navigational profile for a certain flight test, while Figure 6.10 (two additional line plots) explains the velocity and altitude parameters during the test. Both Figures 6.9 and 6.10 were designed around the 10 Hz telemetry data acquired from the airplane. For this test, the autopilot was transitioned from Pilot In Command (PIC) mode to Computer In Command (CIC) mode while the aircraft was heading southeast at a desired airspeed of 20 m/s and a desired altitude of 83 m. Way points were set respectively first (E210m, N200m), second (E0m, N300m), and third (E280m, N200m) from the home position (E0m, N0m). Figure 6.9 illustrates that the plane accurately navigated itself between the waypoints even in the presence of about 3 m/s WNW cross winds. Figure 6.10 shows the altitude and velocity of the plane throughout

it's navigation between way points. GPS speed means ground speed, which measured by GPS receiver. Figure 6.10, in the left-most graph, differentiate between the airspeed and GPS speed. This observed difference is caused by 3 m/s WNW cross winds. Even in the windy conditions, the airplane reasonably maintained the desired altitude and airspeed.

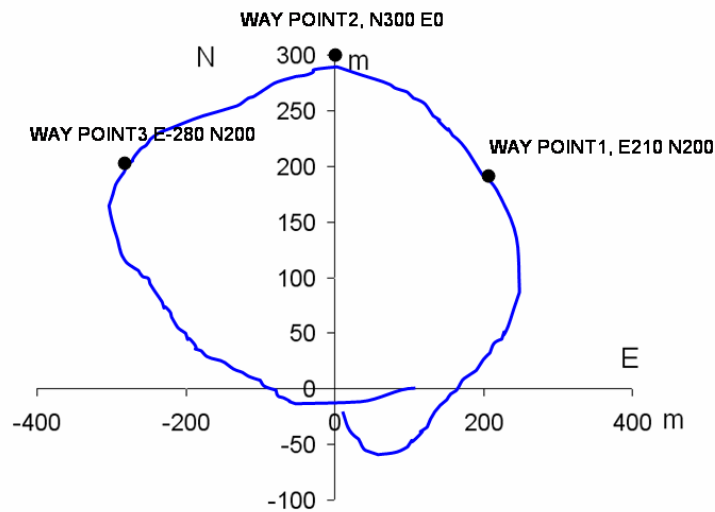


Figure 6.9 Plan form of waypoints flight

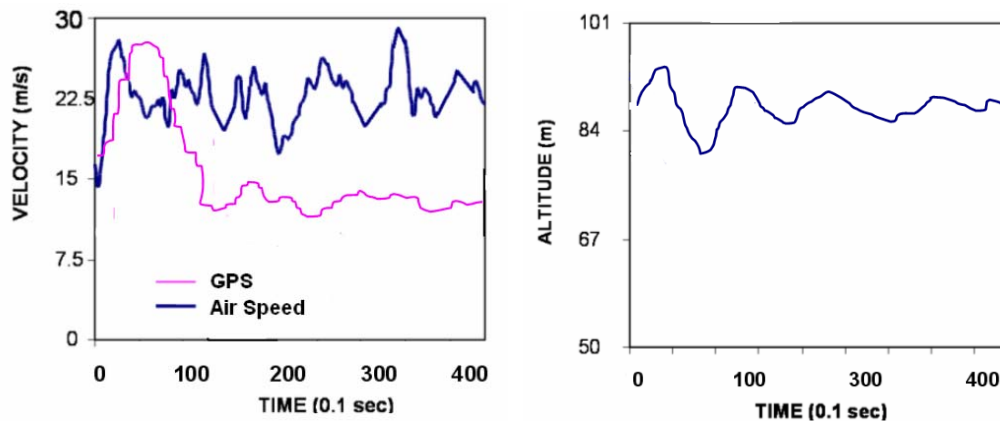


Figure 6.10 Altitude and velocity holding during waypoints navigation

CHAPTER 7 CONCLUSION

7.1 Conclusion

Chapter six showed that the overall airplane performance fits within the imposed design and application requirements. The airplane aerodynamic efficiency was designed to be most efficient at a cruising speed of about 22 m/s. A suitable propulsion system was also installed to be the most efficient at this velocity. However, field tests provided evidence that in order for the airplane to be used for its intended application, RF communication needs to be more reliable. The airplane was designed not only around flight requirements, but also around an inexpensive price range. The plane costs much less than its counterparts and is designed for easy part replacements (modular design). The airplane also proved itself very durable after withstanding three crashes with minimal damage. With these two primary objectives met and more stable RF communication, the airplane would fit the complete criteria of a WSUAV.

7.2 Future Recommendation

Future applications of the airplane will require more research in all areas of the airplane design. Further investigation could result in a smaller airplane platform. Recent progress in technology, specifically in electronics and battery technology, has allowed the construction of MAVs. Similar construction techniques and electrical components could help realize a similar sized WSUAV. This smaller application could allow surveillance of more confined wildlife territories and can also takeoff and land in more restricted areas.

APPENDIX A
LKH2411 AIRFOIL COORDINATES

| point | x | y | point | x | y | point | x | y |
|-------|----------|----------|-------|----------|----------|-------|----------|----------|
| 1 | 1 | -0.01371 | 48 | 0.132932 | 0.061543 | 95 | 0.315474 | -0.04158 |
| 2 | 0.993023 | -0.01098 | 49 | 0.116668 | 0.05934 | 96 | 0.333923 | -0.04108 |
| 3 | 0.980609 | -0.00762 | 50 | 0.100723 | 0.056425 | 97 | 0.353299 | -0.04049 |
| 4 | 0.964456 | -0.00446 | 51 | 0.086553 | 0.053015 | 98 | 0.37023 | -0.03993 |
| 5 | 0.945741 | -0.00142 | 52 | 0.073712 | 0.049315 | 99 | 0.385869 | -0.0394 |
| 6 | 0.926126 | 0.001045 | 53 | 0.062965 | 0.045827 | 100 | 0.402271 | -0.03882 |
| 7 | 0.905582 | 0.003852 | 54 | 0.054102 | 0.04272 | 101 | 0.420701 | -0.03817 |
| 8 | 0.883354 | 0.007311 | 55 | 0.046444 | 0.039854 | 102 | 0.440581 | -0.03747 |
| 9 | 0.861453 | 0.010259 | 56 | 0.039504 | 0.03701 | 103 | 0.461662 | -0.03675 |
| 10 | 0.839938 | 0.012927 | 57 | 0.032713 | 0.033874 | 104 | 0.481523 | -0.03609 |
| 11 | 0.818385 | 0.01604 | 58 | 0.026172 | 0.030382 | 105 | 0.498003 | -0.03555 |
| 12 | 0.796791 | 0.018904 | 59 | 0.020667 | 0.026937 | 106 | 0.511519 | -0.0351 |
| 13 | 0.775058 | 0.021583 | 60 | 0.016335 | 0.023778 | 107 | 0.523261 | -0.03471 |
| 14 | 0.752097 | 0.024937 | 61 | 0.012778 | 0.020786 | 108 | 0.533803 | -0.03436 |
| 15 | 0.728613 | 0.02847 | 62 | 0.009639 | 0.017748 | 109 | 0.54397 | -0.03402 |
| 16 | 0.70568 | 0.031404 | 63 | 0.006828 | 0.014605 | 110 | 0.554316 | -0.03366 |
| 17 | 0.682339 | 0.034245 | 64 | 0.004433 | 0.0115 | 111 | 0.565051 | -0.03329 |
| 18 | 0.661258 | 0.036927 | 65 | 0.002586 | 0.008572 | 112 | 0.576429 | -0.03288 |
| 19 | 0.641863 | 0.040019 | 66 | 0.001304 | 0.005852 | 113 | 0.588938 | -0.03242 |
| 20 | 0.621135 | 0.042572 | 67 | 0.000451 | 0.003235 | 114 | 0.603714 | -0.03187 |
| 21 | 0.598085 | 0.045302 | 68 | 0.00002 | 0.000547 | 115 | 0.62086 | -0.03119 |
| 22 | 0.573893 | 0.048408 | 69 | 0.000158 | -0.00223 | 116 | 0.636771 | -0.03053 |
| 23 | 0.550928 | 0.05164 | 70 | 0.000859 | -0.00501 | 117 | 0.650061 | -0.02996 |
| 24 | 0.527955 | 0.054654 | 71 | 0.002151 | -0.0077 | 118 | 0.662361 | -0.02941 |
| 25 | 0.503786 | 0.057314 | 72 | 0.004067 | -0.01028 | 119 | 0.674718 | -0.02886 |
| 26 | 0.479363 | 0.059872 | 73 | 0.006542 | -0.01279 | 120 | 0.686765 | -0.02831 |
| 27 | 0.456339 | 0.062353 | 74 | 0.009595 | -0.01529 | 121 | 0.698079 | -0.02779 |
| 28 | 0.436393 | 0.064149 | 75 | 0.013555 | -0.01785 | 122 | 0.709302 | -0.02728 |
| 29 | 0.418926 | 0.066133 | 76 | 0.018851 | -0.02042 | 123 | 0.721649 | -0.02673 |
| 30 | 0.400821 | 0.067951 | 77 | 0.025888 | -0.02301 | 124 | 0.736569 | -0.02606 |
| 31 | 0.379964 | 0.069511 | 78 | 0.035371 | -0.02565 | 125 | 0.754253 | -0.02531 |
| 32 | 0.358999 | 0.070561 | 79 | 0.048392 | -0.02814 | 126 | 0.772141 | -0.02458 |
| 33 | 0.339982 | 0.071118 | 80 | 0.063677 | -0.03012 | 127 | 0.789338 | -0.02392 |
| 34 | 0.323013 | 0.071333 | 81 | 0.079958 | -0.03194 | 128 | 0.808227 | -0.02326 |
| 35 | 0.307707 | 0.071328 | 82 | 0.09638 | -0.03385 | 129 | 0.830307 | -0.02253 |
| 36 | 0.294609 | 0.07119 | 83 | 0.111125 | -0.03557 | 130 | 0.853721 | -0.02179 |
| 37 | 0.283199 | 0.070982 | 84 | 0.126634 | -0.0373 | 131 | 0.875302 | -0.0211 |
| 38 | 0.273503 | 0.070747 | 85 | 0.140678 | -0.03873 | 132 | 0.892548 | -0.02054 |

| | | | | | | | | |
|----|----------|----------|----|----------|----------|-----|----------|----------|
| 39 | 0.264198 | 0.070478 | 86 | 0.153734 | -0.03991 | 133 | 0.906408 | -0.02006 |
| 40 | 0.254328 | 0.070151 | 87 | 0.168606 | -0.04098 | 134 | 0.919408 | -0.01959 |
| 41 | 0.242798 | 0.069722 | 88 | 0.186977 | -0.0419 | 135 | 0.933748 | -0.01903 |
| 42 | 0.228557 | 0.069118 | 89 | 0.205449 | -0.04246 | 136 | 0.949578 | -0.01837 |
| 43 | 0.21158 | 0.068269 | 90 | 0.222582 | -0.04271 | 137 | 0.964931 | -0.01756 |
| 44 | 0.194295 | 0.067225 | 91 | 0.239588 | -0.04276 | 138 | 0.979617 | -0.0164 |
| 45 | 0.17794 | 0.066041 | 92 | 0.257023 | -0.04265 | 139 | 0.99249 | -0.015 |
| 46 | 0.162619 | 0.064729 | 93 | 0.276303 | -0.0424 | 140 | 1 | -0.01371 |
| 47 | 0.14829 | 0.063305 | 94 | 0.296582 | -0.04203 | | | |

APPENDIX B
LKH 2411 SIMULATION DATA

| AOA | LKH CI | LKH Cd | NA CI | NA Cd | LKHCm | LKHCI/LKHCd | NACI/NACd | NACm |
|------|---------|---------|--------|---------|---------|-------------|-----------|---------|
| -3 | -0.0235 | 0.00967 | | | | | | |
| -2.5 | 0.0266 | 0.00953 | | | | | | |
| -2 | 0.069 | 0.00182 | 0.0262 | 0.00708 | -0.0381 | 37.91208791 | 3.700565 | -0.0561 |
| -1.5 | 0.1163 | 0.00176 | 0.0787 | 0.00657 | -0.0361 | 66.07954545 | 11.97869 | -0.0553 |
| -1 | 0.1652 | 0.00171 | 0.1302 | 0.00613 | -0.0344 | 96.60818713 | 21.2398 | -0.0541 |
| -0.5 | 0.2084 | 0.00169 | 0.1808 | 0.0058 | -0.0314 | 123.3136095 | 31.17241 | -0.0526 |
| 0 | 0.3022 | 0.00176 | 0.2298 | 0.00563 | -0.027 | 171.7045455 | 40.81705 | -0.0503 |
| 0.5 | 0.4122 | 0.00209 | 0.2834 | 0.00573 | -0.0509 | 197.2248804 | 49.45899 | -0.049 |
| 1 | 0.483 | 0.00238 | 0.3516 | 0.00597 | -0.0537 | 202.9411765 | 58.89447 | -0.0512 |
| 1.5 | 0.5332 | 0.00255 | 0.4032 | 0.00622 | -0.0595 | 209.0980392 | 64.82315 | -0.0541 |
| 2 | 0.6485 | 0.00264 | 0.4991 | 0.0065 | -0.065 | 245.6439394 | 76.78462 | -0.059 |
| 2.5 | 0.6874 | 0.00265 | 0.5483 | 0.00674 | -0.0614 | 259.3962264 | 81.35015 | -0.0576 |
| 3 | 0.7217 | 0.00309 | 0.5975 | 0.00701 | -0.0571 | 233.5598706 | 85.23538 | -0.0563 |
| 3.5 | 0.764 | 0.00342 | 0.6469 | 0.00731 | -0.0542 | 223.3918129 | 88.49521 | -0.0549 |
| 4 | 0.8081 | 0.00376 | 0.6963 | 0.00765 | -0.0515 | 214.9202128 | 91.01961 | -0.0536 |
| 4.5 | 0.8526 | 0.00411 | 0.7459 | 0.00805 | -0.049 | 207.4452555 | 92.65839 | -0.0523 |
| 5 | 0.8958 | 0.00455 | 0.7955 | 0.00852 | -0.0463 | 196.8791209 | 93.36854 | -0.0511 |
| 5.5 | 0.9414 | 0.00492 | 0.8436 | 0.0092 | -0.0441 | 191.3414634 | 91.69565 | -0.0498 |
| 6 | 0.9852 | 0.00538 | 0.8903 | 0.01008 | -0.0415 | 183.1226766 | 88.32341 | -0.0484 |
| 6.5 | 1.0286 | 0.00583 | 0.9356 | 0.01114 | -0.039 | 176.432247 | 83.98564 | -0.0468 |
| 7 | 1.0731 | 0.00626 | 0.9803 | 0.01226 | -0.0366 | 171.4217252 | 79.95922 | -0.0452 |
| 7.5 | 1.108 | 0.00701 | 1.0256 | 0.01331 | -0.0328 | 158.0599144 | 77.05485 | -0.0436 |
| 8 | 1.1423 | 0.00801 | 1.0709 | 0.0143 | -0.0288 | 142.6092385 | 74.88811 | -0.0421 |
| 8.5 | 1.1775 | 0.00899 | 1.1153 | 0.01532 | -0.025 | 130.9788654 | 72.80026 | -0.0404 |
| 9 | 1.2075 | 0.01026 | 1.1579 | 0.01644 | -0.0205 | 117.6900585 | 70.43187 | -0.0384 |
| 9.5 | 1.2424 | 0.01122 | 1.1964 | 0.01781 | -0.0169 | 110.7308378 | 67.17574 | -0.0359 |
| 10 | 1.2665 | 0.01262 | 1.2369 | 0.01889 | -0.0117 | 100.3565769 | 65.47909 | -0.0338 |
| 10.5 | 1.2913 | 0.01373 | 1.2647 | 0.0208 | -0.0066 | 94.04952658 | 60.80288 | -0.0299 |
| 11 | 1.3168 | 0.01493 | 1.2973 | 0.02198 | -0.002 | 88.19825854 | 59.02184 | -0.0266 |
| 11.5 | 1.3319 | 0.01678 | 1.3235 | 0.02352 | 0.0033 | 79.37425507 | 56.27126 | -0.0229 |
| 12 | 1.3555 | 0.01845 | 1.3303 | 0.02658 | 0.0068 | 73.46883469 | 50.04891 | -0.0174 |
| 12.5 | 1.3771 | 0.02041 | 1.3527 | 0.02869 | 0.0097 | 67.47182754 | 47.14883 | -0.0143 |
| 13 | 1.3886 | 0.0234 | 1.3689 | 0.03147 | 0.0123 | 59.34188034 | 43.49857 | -0.0114 |
| 13.5 | 1.4071 | 0.02635 | 1.3823 | 0.03472 | 0.0136 | 53.40037951 | 39.81279 | -0.0091 |
| 14 | 1.424 | 0.02966 | 1.3902 | 0.03878 | 0.0143 | 48.01078894 | 35.84838 | -0.0075 |
| 14.5 | 1.4274 | 0.03461 | 1.3788 | 0.04523 | 0.0143 | 41.24241549 | 30.48419 | -0.0059 |
| 15 | 1.4426 | 0.0386 | 1.3835 | 0.05041 | 0.0141 | 37.37305699 | 27.44495 | -0.006 |
| 15.5 | 1.4342 | 0.04532 | 1.3806 | 0.05682 | 0.0129 | 31.64607237 | 24.29778 | -0.0068 |
| 16 | 1.4318 | 0.05167 | 1.3724 | 0.06428 | 0.0116 | 27.71047029 | 21.35034 | -0.0085 |
| 16.5 | 1.4171 | 0.05982 | 1.3599 | 0.07284 | 0.0093 | 23.68940154 | 18.66969 | -0.0112 |
| 17 | 1.3834 | 0.07118 | 1.3432 | 0.08251 | 0.0051 | 19.43523462 | 16.27924 | -0.0148 |
| 17.5 | 1.3595 | 0.08195 | 1.3227 | 0.09327 | 0.0009 | 16.58938377 | 14.18141 | -0.0194 |
| 18 | 1.3269 | 0.09475 | 1.2986 | 0.10516 | -0.0046 | 14.00422164 | 12.3488 | -0.0249 |

| | | | | | | | | |
|------|--------|---------|--------|---------|---------|-------------|----------|---------|
| 18.5 | 1.2909 | 0.10879 | 1.27 | 0.11849 | -0.0111 | 11.86598033 | 10.7182 | -0.0316 |
| 19 | 1.2579 | 0.12244 | 1.2376 | 0.13328 | -0.0178 | 10.2736034 | 9.285714 | -0.0396 |
| 19.5 | 1.2282 | 0.13578 | 1.1889 | 0.15298 | -0.0247 | 9.045514803 | 7.771604 | -0.0512 |

APPENDIX C
EH 00/90 AIRFOIL COORDINATES

| x | y | x | y | x | y |
|---------------------|----------|--------------------------|--------|--------|---------|
| 100 | 0 0.0000 | 23.209 | 4.415 | 25.912 | -4.474 |
| 99.901 | 0.004 | 20.611 | 4.323 | 28.711 | -4.5 |
| 99.606 | 0.018 | 18.129 | 4.198 | 31.594 | -4.495 |
| 99.114 | 0.046 | 15.773 | 4.039 | 34.549 | -4.46 |
| 98.429 | 0.092 | 13.552 | 3.847 | 37.565 | -4.396 |
| 97.553 | 0.158 | 11.474 | 3.624 | 40.631 | -4.306 |
| 96.489 | 0.243 | 9.549 | 3.37 | 43.733 | -4.191 |
| 95.241 | 0.345 | 7.784 | 3.087 | 46.861 | -4.054 |
| 93.815 | 0.463 | 6.185 | 2.778 | 50 | -3.895 |
| 92.216 | 0.597 | 4.759 | 2.445 | 53.139 | -3.716 |
| 90.451 | 0.748 | 3.511 | 2.094 | 56.267 | -3.526 |
| 88.526 | 0.916 | 2.447 | 1.726 | 59.369 | -3.32 |
| 86.448 | 1.1 | 1.571 | 1.35 | 62.435 | -3.104 |
| 84.227 | 1.297 | 0.886 | 0.984 | 65.451 | -2.879 |
| 81.871 | 1.505 | 0.394 | 0.623 | 68.406 | -2.648 |
| 79.389 | 1.724 | 0.099 | 0.289 | 71.289 | -2.415 |
| 74.088 | 2.181 | 0 | 0 | 74.088 | -2.181 |
| 71.289 | 2.415 | 0.099 | -0.289 | 76.791 | -1.95 |
| 68.406 | 2.648 | 0.394 | -0.623 | 79.389 | -1.724 |
| 65.451 | 2.879 | 0.886 | -0.984 | 81.871 | -1.505 |
| 62.435 | 3.104 | 1.571 | -1.35 | 84.227 | -1.297 |
| 59.369 | 3.32 | 2.447 | -1.726 | 86.448 | -1.1 |
| 56.267 | 3.526 | 3.511 | -2.094 | 88.526 | -0.916 |
| 53.139 | 3.716 | 4.759 | -2.445 | 90.451 | -0.748 |
| 50 | 3.895 | 6.185 | -2.778 | 92.216 | -0.597 |
| 46.861 | 4.054 | 7.784 | -3.087 | 93.815 | -0.463 |
| 43.733 | 4.191 | 9.549 | -3.37 | 95.241 | -0.345 |
| 40.631 | 4.306 | 11.474 | -3.624 | 96.489 | -0.243 |
| 37.565 | 4.396 | 13.552 | -3.847 | 97.553 | -0.158 |
| 34.549 | 4.46 | 15.773 | -4.039 | 98.429 | -0.092 |
| 31.594 | 4.495 | 18.129 | -4.198 | 99.114 | -0.046 |
| 28.711 | 4.5 | 20.611 | -4.323 | 99.606 | -0.018 |
| 25.912 | 4.474 | 23.209 | -4.415 | 99.901 | -0.004 |
| max thickness 9.00% | | max thickness 29.7% code | | 100 | 0 0.000 |

LIST OF REFERENCES

1. Reed Siefert Christiansen, "Design of an Autopilot for Small Unmanned Aerial Vehicles," M.S. thesis, Electrical and Computer Engineering, Brigham Young University, pp.2-4, August 2004.
2. J. Pike, "Dragon Eye" Intelligence Resources. 2000. GlobalSecurity.org. <http://www.globalsecurity.org/intell/systems/dragon-eye.htm>, 21 December 2003.
3. Robert Bowman, "Large Unmanned Vehicles," volume 9, Shephard Unmanned Vehicles Journal, pp.55-56, November 2004.
4. David Rocky, "Tactical Unmanned Aerial Vehicles," volume 18, AUVSI magazine, pp.28-30, August 2004.
5. Sewoong Jung, "Design and Development of Micro Air Vehicle: Test Bed for Vision-Based Control," M.S. thesis, Mechanical and Aerospace Engineering Department, University of Florida, pp. 3-10, August 2004.
6. R. Albertani, P. Barnswell, F. Boria, D. Claxton, J. Clifton, J. Cocquyt, A. Crespo, C. Francis, P. Ifju, B. Johnson, S. Jung, K. Lee, and M. Morton, "University of Florida Biologically Inspired Micro Air Vehicles," April 2004.
7. A. Parsch, "AeroVironment FQM-151 Pointer," Directory of U.S. Military Rockets and Missiles. 2004. Designation-Systems.Net. <http://www.designation-systems.net/dusrm/m-151.html>, 24 March 2004.
8. N. Newcome, "News Room," volume 10, Unmanned Aerial Vehicles Journal, SRA International, Inc., pp.3-5, 4 October 2003.
9. Darrin M. Thome and Timonthy M. Thome, "Radio-Controlled Model Airplanes: Inexpensive Tools for Low-Level Aerial Photography," Wildlife Society Bulletin, pp.343-345, April 2004.
10. Scott M. Bowman and Peter C William, "Radio-Controlled Airplanes for Aerial and Ground survey," volume 14, Wildlife Society Bulletin, pp.347-348, April 2002.
11. George Pierce Jones, IV, "The Feasibility of Using Small Unmanned Aerial Vehicles for Wildlife Research," M.S. thesis, Wildlife and Ecology Conservation, University of Florida, pp. 20-40, August 2003.

12. Daniel P. Raymer, *Aircraft Design: A Conceptual Approach*, second edition, AIAA Education series, Washington, 1992.
13. J. Pike, "Dragon Eye," Intelligence resources. 2000. GlobalSecurity.org.
<http://www.globalsecurity.org/intell/systems/dragon-eye.htm>, December 2003.
14. J. D. Anderson, *Introduction to Flight*, fourth edition, WCB/McGraw-Hill, pp.707 - 708, Boston, 2000.
15. Jaewoo Lee and Youngjae Lee, *Aircraft Conceptual Design: Aviation Education*, Aircraft Design and Education Center ,pp.246-249, Seoul, November 2003.
16. Dragos Viieru, Roberto Albertani, Wei Shyy, and Peter Ifju, "Effect of Tip Vortex on Wing Aerodynamics of Micro Aerial Vehicles," 22nd AIAA Conference paper, Reno, August 2004.
17. Aeronautic Analysis, "Aircraft Design and Analysis," monthly technical bulletin volume 21, pp.13-15, September 2001.
18. J. D. Anderson, *Aircraft Performance and Design*, WCB/McGraw-Hill, Boston, 1998.
19. A. Lennon, *The Basics of R/C Model Aircraft Design*, Air Age Inc., pp.10-14, Ridgefield, 1999.
20. Peterson Vizmuller, *Electric Design Guide: Systems and Power*, Airtech House Inc, Boston, June 1995.
21. J. M. Grasmeyer and M. T. Keennon, "Development of the Black Widow Micro Air Vehicle," AIAA paper, San Francisco, January 2001.

BIOGRAPHICAL SKETCH

Kyuhoo Lee was born in Seoul, Korea, on May 15, 1971. He received his bachelor's degree in aerospace engineering from Kunkuk University, Seoul, Korea, in Feb 2001. He has since worked for Korean Air lines as a mechanical engineer for 5 years and Korean Institute of Science and Technologies (KIST) for 2 years as a MAV researcher.

In August 2002, he joined the University of Florida to pursue a Master of Science in mechanical and aerospace engineering. He worked as a graduate research assistant in the MAV Laboratory under the advisement of Dr. Peter Ifju. He won the MAV competition held in Arizona in April 2004. His research interests include MAV and Mini UAV.